Elm1 kinase activates the spindle position checkpoint kinase Kin4

Ayse Koca Caydasi, Bahtiyar Kurtulmus, Maria I.L. Orrico, Astrid Hofmann, Bashar Ibrahim, and Gislene Pereira

German Cancer Research Center, DKFZ-ZMBH Alliance, Molecular Biology of Centrosomes and Cilia, 69120 Heidelberg, Germany

Budding yeast asymmetric cell division relies upon the precise coordination of spindle orientation and cell cycle progression. The spindle position checkpoint (SPOC) is a surveillance mechanism that prevents cells with misoriented spindles from exiting mitosis. The cortical kinase Kin4 acts near the top of this network. How Kin4 kinase activity is regulated and maintained in respect to spindle positional cues remains to be established. Here, we show that the bud neck–associated kinase Elm1 participates in Kin4 activation and SPOC signaling by phosphorylating a conserved residue within the activation loop of Kin4. Blocking Elm1 function abolishes Kin4 kinase activity in vivo and eliminates the SPOC response to spindle misalignment. These findings establish a novel function for Elm1 in the coordination of spindle positioning with cell cycle progression via its control of Kin4.

Introduction

For asymmetric cell division, the correct alignment of the mitotic spindle along the polarity axis of a cell is crucial to ensure both the fidelity of chromosome segregation and cell fate determination. In *Saccharomyces cerevisiae* (budding yeast), the axis of cell polarity is established at G1–S transition, when the daughter cell (the bud) starts to emerge (Casamayor and Snyder, 2002). The site of bud emergence, named the bud neck, dictates the site of cytokinesis in the subsequent mitosis. Therefore, budding yeast cells must align the mitotic spindle parallel to the mother–bud axis to ensure that one chromosome set remains in the mother cell and the other passes through the bud neck into the daughter before cytokinesis completes cell fission. If the spindle is misoriented in anaphase, a surveillance mechanism named the spindle position checkpoint (SPOC) comes into play to delay mitotic exit until the spindle resumes the correct orientation. The SPOC imposes this delay by inactivating the mitotic exit network (MEN; Lew and Burke, 2003; Fraschini et al., 2008).

The MEN is a GTPase-driven signal transduction cascade that promotes the full activation of the conserved phosphatase that drives mitotic exit, Cdc14 (Bardin and Amon, 2001). Activation of the GTPase Tem1 constitutes the main switch that initiates MEN signaling. Tem1 is inhibited by the GTPase-activating protein (GAP) composed of a bipartite complex of Bub2 and Bfa1 (Geymonat et al., 2002). The GAP activity of Bub2–Bfa1 is regulated by the action of the polo-like kinase Cdc5 and Kin4. In an undisturbed anaphase, when the spindle is correctly aligned, Cdc5 inactivates the Bub2–Bfa1 GAP through phosphorylation of Bfa1 (Hu et al., 2001; Geymonat et al., 2003). This drives MEN activation. However, if the cytoplasmic microtubules fail to establish the correct orientation of the spindle, Kin4 kinase phosphorylates Bfa1 and thereby blocks the inhibitory phosphorylation of Bfa1 by Cdc5 such that cells are now unable to activate the MEN even if Cdc5 is active (D'Aquino et al., 2005; Pereira and Schiebel, 2005; Maekawa et al., 2007). Thus, Bub2–Bfa1 together with its regulators Cdc5 and Kin4 constitute the SPOC.

Localization of SPOC components changes upon spindle misalignment. In an unperturbed cell cycle, Tem1 and Bub2–Bfa1 localize preferentially to the bud ward–directed spindle pole body (SPB; yeast centrosome; Bardin et al., 2000; Pereira et al., 2000). Kin4 kinase associates with both the mother cell cortex and the SPB that stays within this mother cell (mSPB). In late anaphase, Kin4 binds to the bud neck (D'Aquino et al., 2005; Pereira and Schiebel, 2005). Interestingly, when the spindles are misaligned, Bub2–Bfa1, Kin4, and Tem1 all bind symmetrically to both SPBs (Pereira et al., 2000; Pereira and

Correspondence to Gislene Pereira: g.pereira@dkfz.de

M.I.L. Orrico's present address is Johnson & Johnson Group of Consumer Companies, 12240-907 Sao Jose dos Campos, Brazil.

Abbreviations used in this paper: GAP, GTPase-activating protein; MEN, mitotic exit network; SPB, spindle pole body; SPOC, spindle position checkpoint.

The Rockefeller University Press $30.00
J. Cell Biol. Vol. 190 No. 6 975–989
www.jcb.org/cgi/doi/10.1083/jcb.201006151

Schiebel, 2001; Molk et al., 2004). The turnover rate of Tem1 at the SPBs is high and is independent of the status of spindle orientation (Molk et al., 2004; Caydasi and Pereira, 2009). In contrast, Bub2 and Bfa1 bind stably to the daughter cell SPB (dSPB) when the spindle is properly aligned. However, upon checkpoint activation, the dynamics with which Bub2–Bfa1 turns over at the SPBs increase dramatically (Caydasi and Pereira, 2009; Monje-Casas and Amon, 2009). This change in binding dynamics is triggered by Kin4-dependent phosphorylation of Bfa1 and plays a key role in SPOC function (Caydasi and Pereira, 2009).

Most studies to date have focused upon the regulation of the Bub2–Bfa1 GAP complex and largely ignored Kin4 regulation. A recent study suggested that localization of Kin4 to the cortex and SPB is regulated by the activity of the protein phosphatase 2A (PP2A) subunit Rts1 (Chan and Amon, 2009); however the underlying molecular mechanisms remain unclear. Here, we find that the kinase Elm1 (elongation morphology 1; Blacketer et al., 1993) promotes the activation of the catalytic activity of Kin4. Elm1 is a bud neck–associated kinase that plays essential roles in controlling bud neck integrity, cell cycle progression, and the yeast SNF1–AMP-activated protein kinase (AMPK) pathway that regulates cell homeostasis (Edgington et al., 1999; Sreenivasan and Kellogg, 1999; Bouquin et al., 2000; Hong et al., 2003; Sutherland et al., 2003; Hedbacker and Carlson, 2008). We identified *ELM1* in a genetic screen for positive regulators of Kin4. In *elm1Δ* cells, Kin4 kinase activity was drastically reduced, and localization of Kin4 to the cell cortex was diminished. Consistently, *elm1Δ* cells were SPOC deficient. In vitro and in vivo data established that Elm1 phosphorylates Kin4 at the conserved threonine 209 within the activation loop. Impairment of Kin4 phosphorylation at threonine 209 causes SPOC deficiency. These findings have established a novel function for Elm1 in acting upstream of Kin4, in the control of SPOC function.

Results

Loss of *ELM1* function rescues the lethality of *KIN4* overexpression

Overexpression of *KIN4* kills cells because it drives the constitutive inactivation of the MEN by the Bub2–Bfa1 GAP complex and thus blocks the cell cycle at the end of anaphase (D'Aquino et al., 2005). As a consequence, deletion of either *BUB2* or *BFA1* relieves MEN inhibition and allows growth of cells overproducing Kin4. To identify additional components involved in Kin4 regulation, we performed a genetic screen to identify genes whose inactivation rescued the lethality of *KIN4* overexpression. These genes were expected to be involved in either the activation of Kin4 or to function downstream or parallel to Kin4 in MEN signaling. Using random UV irradiation, we mutated cells carrying two chromosomally integrated *KIN4* copies under control of the inducible Gal1 and Met25 promoters. Only mutants that were able to grow under both Gal1-*KIN4*– and Met25-*KIN4*–inducing conditions were considered for further analysis. The mutated genes were identified by their ability to complement the Gal1-*KIN4* growth phenotype.

In addition to the known SPOC component *BUB2*, we identified the bud neck–associated kinase *ELM1* (Blacketer et al., 1993) and the PP2A regulatory subunit *RTS1* (Evangelista et al., 1996; Shu et al., 1997) as potential Kin4 regulators. Single deletion analysis confirmed that the rescue of *KIN4* overexpression toxicity was a consequence of loss of *ELM1* function (Fig. 1 A). Interestingly, deletion of *ELM1* suppressed the growth of Gal1-*KIN4* cells more effectively than the deletion of *RTS1* (Fig. 1 A). Cells in which *ELM1* was replaced with a catalytically inactive "kinase-dead" *ELM1* allele (*elm1-kd*, *elm1-K117R*; Koehler and Myers, 1997) were also able to grow when *KIN4* was overexpressed. This data shows that Elm1 kinase activity contributes to the toxicity arising from Kin4 overproduction (Fig. 1 B). Rts1 was recently shown to be a SPOC component (Chan and Amon, 2009). We therefore focused our studies upon understanding the molecular basis of Elm1 control of Kin4 function.

ELM1 deletion rescues *KIN4* overexpression toxicity in the absence of *SWE1*

Elm1 functions at the top of a cascade by which the septin kinases Hsl1 and Gin4 negatively regulate Swe1 (Barral et al., 1999; Sreenivasan and Kellogg, 1999; Bouquin et al., 2000). Swe1 controls cellular morphogenesis by inhibiting the activity of the budding yeast Cdk1 (Lew and Reed, 1995; Sia et al., 1996). Cells lacking *ELM1*, *HSL1*, or *GIN4* exhibit elongated cell morphology because Swe1 kinase is no longer restrained and its activity rises beyond normal levels. Deletion of *SWE1* therefore rescues the elongated bud morphology of *elm1Δ* and *hsl1Δ gin4Δ* cells (Barral et al., 1999; Edgington et al., 1999; Sreenivasan and Kellogg, 1999).

This functional relationship between Elm1 and Swe1 raises the possibility that Elm1 rescues the lethality of *KIN4* overexpression as an indirect consequence of the hyperactivation of Swe1. If this were to be the case, *elm1Δ swe1Δ* Gal1-*KIN4* cells should be unable to grow in the presence of high levels of Kin4. However, deletion of *SWE1* in *elm1Δ* cells did not restore the lethality of *KIN4* overexpression. Moreover, the *hsl1Δ gin4Δ* double mutant was unable to grow when Kin4 was overproduced (Fig. 1 C). Finally, deletion of any of the other kinases that are positively regulated by Elm1 (Hsl1, Gin4, Snf1, and Cla4; Mortensen et al., 2002; Hong et al., 2003; Sutherland et al., 2003; Asano et al., 2006; Szkotnicki et al., 2008) also failed to rescue the toxicity of *KIN4* overexpression (Fig. 1 C). Thus, the function of Elm1 in suppressing the lethality of high Kin4 kinase activity is independent of its previously established roles in the control of Swe1 and other kinases.

Bfa1 localization and phosphorylation is altered by removal of Elm1

Next, we used Bfa1 localization and phosphorylation as a readout to compare the competence of Kin4 function of *elm1Δ*, *rts1Δ*, and wild-type cells. *KIN4* overexpression increases Bfa1 turnover at the SPBs, leading to symmetric, but less intense association of Bfa1 with SPBs (Caydasi and Pereira, 2009).

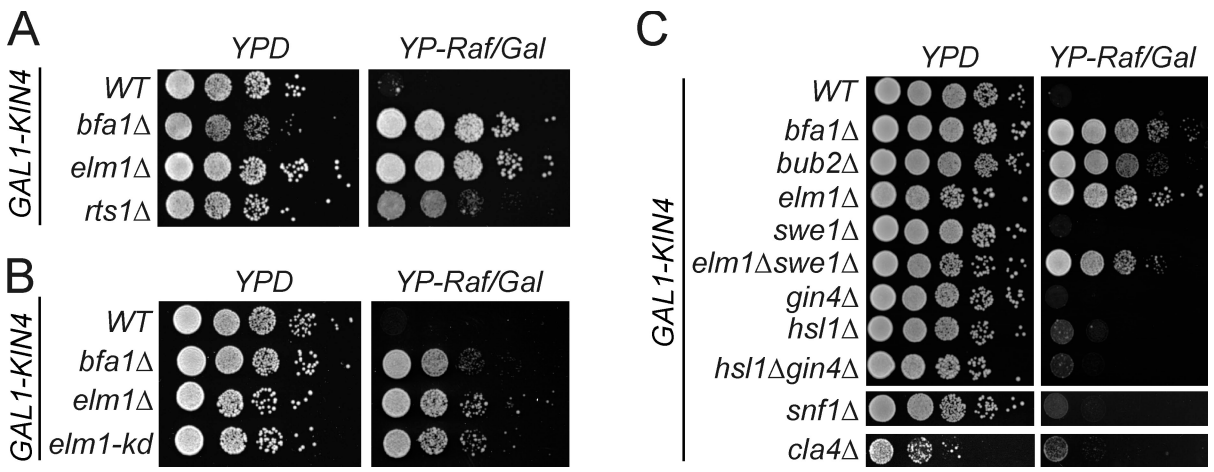

Figure 1. **Deletion of *ELM1* rescues Gal1-*KIN4* overexpression.** Serial dilutions of the indicated strains were spotted on plates under Gal1-repressing (YPD) or -inducing (YP-Raf/Gal) conditions.

To investigate the SPB-binding behavior of Bfa1, *KIN4* expression was induced in wild-type, *elm1Δ*, and *rts1Δ* cells that had been arrested at metaphase by depletion of the APC-activating subunit Cdc20 (Shirayama et al., 1998). Kin4 accumulated to similar levels in all three strains (data not shown). As expected, in wild-type cells, Bfa1-GFP localization became symmetric upon overproduction of Kin4, and the intensity of Bfa1-GFP at the SPBs decreased (Fig. 2, A and D, GAL). The Bfa1-GFP signal of *rts1Δ* responded in a similar way to that of the wild-type controls (Fig. 2, B and D). In contrast, localization of Bfa1-GFP did not significantly change in *elm1Δ* cells despite the elevation of *KIN4* levels (Fig. 2, C and D), which implies that Kin4 was not fully functional in the absence of Elm1.

During anaphase, phosphorylation of Bfa1 by Cdc5 inhibits the Bfa1-Bub2 GAP (Hu et al., 2001). In response to spindle alignment defects or microtubule depolymerization by nocodazole, Bfa1 persists in a hypophosphorylated state because Kin4 kinase blocks the ability of Cdc5 to execute this inactivating phosphorylation of Bfa1. Thus, deletion of *KIN4* results in Cdc5-dependent Bfa1 hyperphosphorylation in nocodazole-treated cells, despite SPOC activation (D'Aquino et al., 2005; Pereira and Schiebel, 2005; Maekawa et al., 2007). To determine the phosphorylation status of Bfa1, cells were first arrested in G1 phase of the cell cycle by α-factor–induced arrest and allowed to progress out of this G1 block in the presence of nocodazole (Fig. 2 E). The accumulation of the mitotic cyclin Clb2 and cells with large buds were used as reference marks to monitor the extent to which the lack of microtubules blocked mitotic progression. *bub2Δ* cells escaped the nocodazole block and continued cell cycle progression without hyperphosphorylation of Bfa1 (Fig. 2 E). In contrast, the high levels of Clb2 and accumulation of late anaphase cells (large budded cells) indicated that *elm1Δ* cells were able to maintain the metaphase arrest in an identical fashion to *rts1Δ*, *kin4Δ*, and wild-type cells. Strikingly, hyperphosphorylated forms of Bfa1 accumulated even more pronouncedly in *elm1Δ* compared with *kin4Δ* strains (Fig. 2 E). Collectively, these results establish that deletion of *ELM1* phenocopies *kin4Δ* in a phenotype that is distinct from that arising from deletion of *RTS1*.

elm1Δ cells are unable to engage the SPOC

To investigate SPOC proficiency in the absence of *ELM1*, we used *kar9Δ* cells. Kar9 is a component of a pathway that stabilizes the interaction of cytoplasmic microtubules with the bud neck (for review see Segal and Bloom, 2001). Cells lacking *KAR9* show a higher frequency of spindle alignment defects at elevated temperatures (Miller and Rose, 1998). These *kar9Δ* cells, which have spindle alignment defects, arrest in anaphase because of SPOC activation, whereas cell cycle progression is unaffected in cells with correct spindle orientation (Bloecher et al., 2000; Pereira et al., 2000). We used GFP-labeled tubulin (*GFP-TUB1*) to visualize microtubule organization. SPOC-deficient cells exit mitosis and disassemble their spindles even when the anaphase spindle is misaligned in the mother cell (Pereira and Schiebel, 2005). To compare the SPOC proficiency of *elm1Δ kar9Δ* and *rts1Δ kar9Δ* cells, we determined the length of anaphase during normal cell cycle progression and when the spindle was misaligned by live cell imaging (anaphase duration; Fig. 3, A and B). Cells deleted of *KAR9* were especially useful for this analysis, as cells with both aligned and misaligned spindles were frequently observed within the same population under normal growth conditions. The anaphase duration of *GFP-TUB1 kar9Δ* cells was calculated as the time from the onset of spindle elongation until spindle breakdown. When the spindle was properly aligned, anaphase of cells lacking *KAR9* took ∼20 min. However, cells with misaligned spindles remained arrested with intact anaphase spindles for at least 1 h (Fig. 3, A and B). This arrest was relieved only when spindles established correct alignment during the observation. As expected, *kar9Δ bfa1Δ* and *kar9Δ kin4Δ* cells exited mitosis with an anaphase length of ∼20 min regardless of the orientation of the mitotic spindle (Fig. 3 B). Likewise, *kar9Δ elm1Δ* cells broke their aligned or misaligned spindles with a similar timing (∼24 min) after anaphase onset (Fig. 3 B). *kar9Δ rts1Δ* cells were also unable to maintain the late anaphase arrest upon spindle misalignment. However, the anaphase duration of *kar9Δ rts1Δ* cells with spindle misalignment was significantly longer than that of *kar9Δ rts1Δ* cells with properly aligned spindles. This may arise from the multiple functions of Rts1 in mitosis

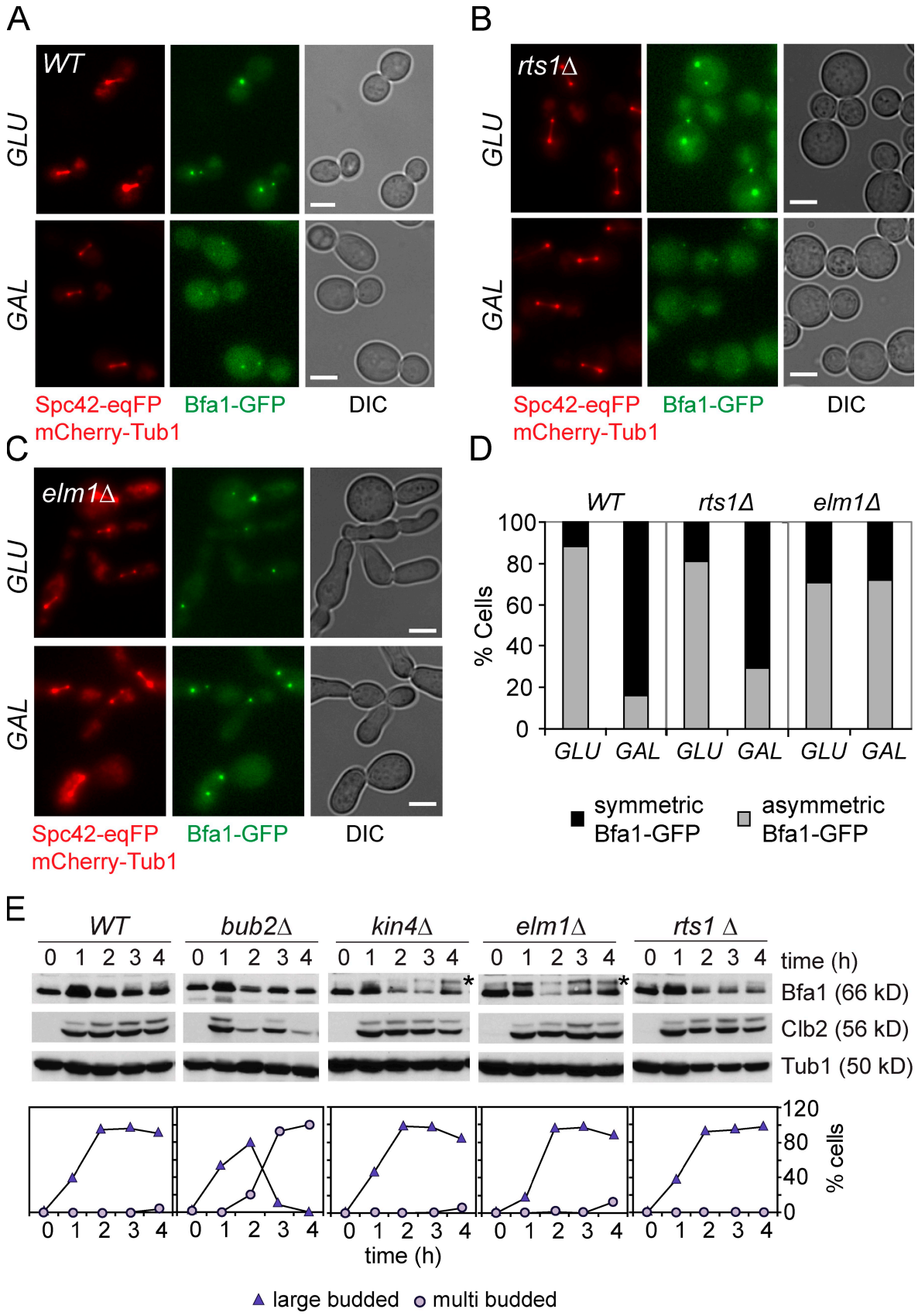

Figure 2. **Bfa1 localization and phosphorylation in *elm1Δ* and *rts1Δ* cells.** (A–C) Met3-*CDC20* Gal1-*KIN4 SPC42-eqFP mCherry-TUB1* cells were arrested in metaphase by Cdc20 depletion followed by the addition of galactose (GAL, induction of Gal1-*KIN4*) or glucose (GLU, repression of Gal1-*KIN4*) for 3 h. Spc42 served as an SPB marker. Localization of Bfa1-GFP at SPBs was inspected after fixing the cells with paraformaldehyde. Bars, 3 µm. (D) Quantification of A–C. Bfa1-GFP was considered symmetric if equally bound to both SPBs and asymmetric if strongly bound to one of the two SPBs. (E) The indicated

A

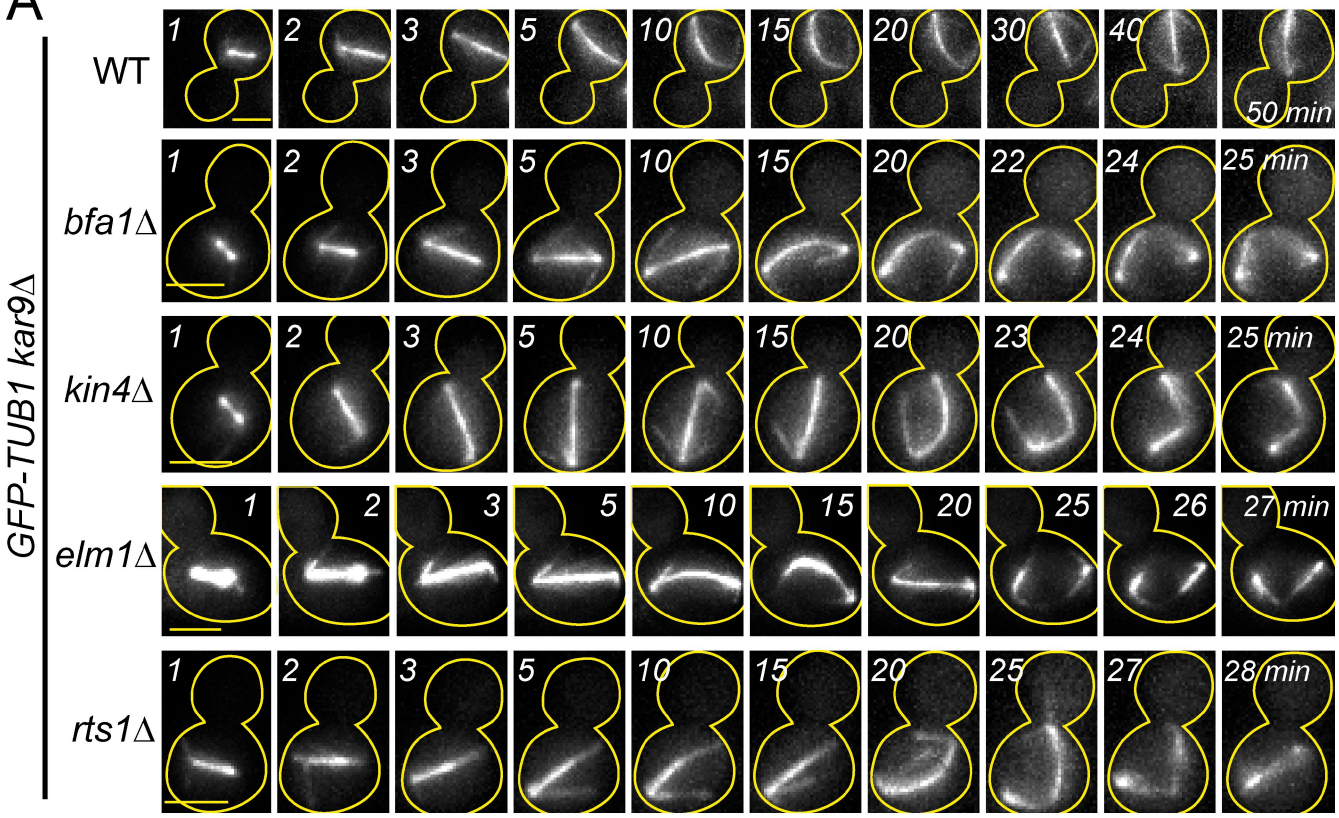

B

Cell type	Spindle alignment status	N	Anaphase duration (min)	
WT	*Aligned*	21	20 ± 3	*
	Misaligned	24	> 60	
		1	33	
bfa1Δ	*Aligned*	13	20 ± 4	
	Misaligned	17	21 ± 7	
kin4Δ	*Aligned*	18	22 ± 4	
	Misaligned	12	24 ± 3	
elm1Δ	*Aligned*	14	23 ± 4	
	Misaligned	9	25 ± 5	
rts1Δ	*Aligned*	54	26 ± 4	*
	Misaligned	12	31 ± 6	

Figure 3. ***elm1Δ* cells are SPOC deficient.** (A) Representative still images of a time-lapse series showing GFP-tubulin in *kar9Δ* cells with misaligned spindles. Approximate cell outlines were drawn considering the cell morphologies. Bars, 3 μm. (B) Comparison of anaphase duration (mean ± SD) between cells with normal and misaligned spindles. Asterisks indicate significant differences between the two indicated samples (*t* test, $P < 0.05$). N, number of the cells inspected.

strains were arrested at G1 phase with α-factor and released in nocodazole-containing media. Bfa1 and Clb2 levels were determined by immunoblotting at the indicated times. Tub1 served as loading control. Asterisks indicate hyperphosphorylated Bfa1 forms. The percentage of large- and multibudded cells was plotted versus time.

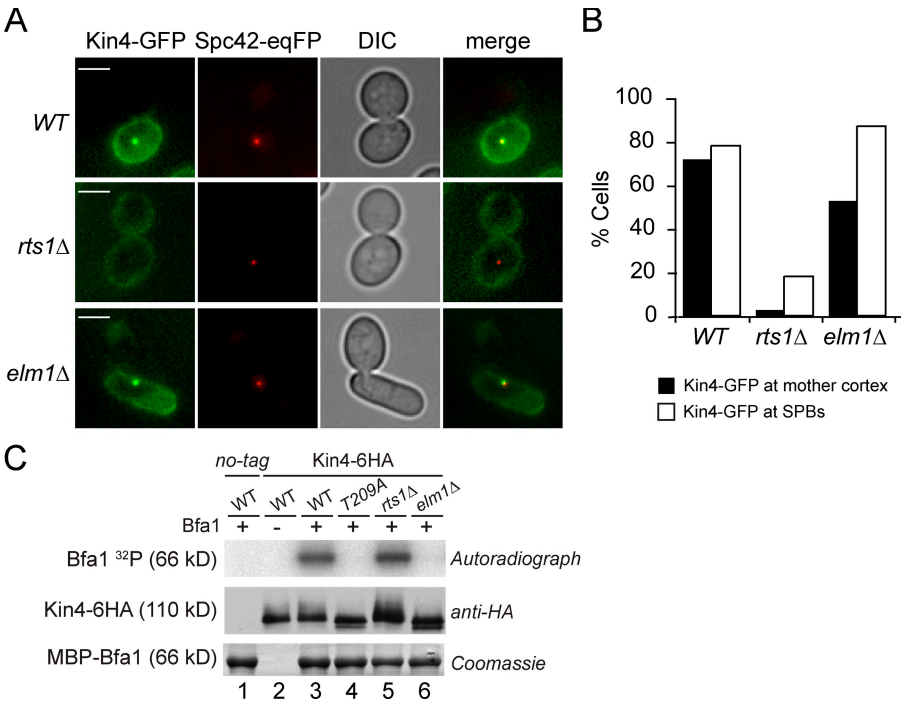

Figure 4. **Localization and activity of Kin4 in *elm1Δ* cells.** (A) Kin4-GFP localization in nocodazole-arrested cells. Spc42-eqFP served as an SPB marker. Images were taken without fixation. Note that the two SPBs collapse, forming a large single eqFP signal, due to depolymerization of the microtubules by nocodazole. Bars, 3 µm. (B) Quantification of A showing one representative experiment out of three; 100–150 cells were counted per sample. (C) In vitro kinase assay using immunoprecipitated Kin4-6HA (lanes 2, 3, 5, and 6) or Kin4-T209A-6HA (lane 4) from cycling cultures of wild type (WT), *rts1Δ*, or *elm1Δ* cells as indicated. Nontagged Kin4 (lane 1) was used as a control for contaminating kinases. Kin4-6HA was detected by immunoblotting (anti-HA). MBP-Bfa1 was used as a substrate (Coomassie staining). Incorporation of the ^{32}P isotope was determined by autoradiography. Note that a 66-kD degradation product of MBP-Bfa1 was phosphorylated efficiently by Kin4-6HA as described in Maekawa et al. (2007). Plus and minus represent the presence and the absence of MBP-Bfa1. Kin4 did not phosphorylate MBP alone (Maekawa et al., 2007; not depicted).

(Shu et al., 1997). These data suggest that Elm1 is essential for the function of the SPOC.

Kin4 association with the cell cortex was decreased in *elm1Δ* cells

Binding of Kin4 to the cortex and SPB is important for SPOC function (Maekawa et al., 2007). We therefore asked whether Elm1 affected this aspect of Kin4 function. The localization of Kin4-GFP was monitored after treatment with nocodazole to increase the proportion of cells with Kin4 at SPBs (Pereira and Schiebel, 2005). Strains also carried the SPB protein Spc42 (Donaldson and Kilmartin, 1996), tagged with the red fluorescent protein eqFP. Kin4-GFP localized to the mother cell cortex and SPBs of wild-type cells (Fig. 4, A and B). As reported previously, deletion of *RTS1* drastically reduced the recruitment of Kin4-GFP to both the SPB and cortex (Fig. 4 A; Chan and Amon, 2009). Interestingly, a higher percentage of *elm1Δ* cells showed reduced cortical Kin4-GFP, whereas Kin4-GFP association with SPBs resembled that seen in wild-type controls. Furthermore, in 80% of *elm1Δ* cells showing diminished association of Kin4-GFP with the cortex, the Kin4-GFP that did associate was more concentrated at the tip of the cell. This type of localization was likely caused by hyperactivation of Swe1, as *SWE1* deletion eliminated this heterogeneity of Kin4-GFP association with the cortex in *elm1Δ* cells (unpublished data). Thus, Elm1 is required for the proper recruitment of Kin4 to the cortex.

Elm1 is required for Kin4 kinase activity

To assess the impact of Elm1 upon the kinase activity of Kin4, we measured Kin4-specific kinase activity using Kin4-6HA enriched from yeast cell lysates and purified MBP-Bfa1 as substrate (Fig. 4 C; Maekawa et al., 2007). Similar levels of Kin4-6HA–specific kinase activity were detected in wild-type and *rts1Δ* cells (Fig. 4 C, lanes 3 and 5). The phosphorylation of MBP-Bfa1 arose from Kin4-6HA and no other contaminant kinases because MBP-Bfa1 was not phosphorylated if the anti-HA beads had been incubated with lysates of *KIN4* rather than *KIN4-6HA* cells (Fig. 4 C, no-tag control, lane 1). Deletion of *ELM1* diminished Kin4-6HA kinase activity to levels comparable to those observed for the inactive mutant Kin4-T209A-6HA (D'Aquino et al., 2005; Maekawa et al., 2007), in which threonine 209 was substituted to alanine (Fig. 4 C, lanes 4 and 6). These data establish that Elm1 regulates the kinase activity of Kin4.

Elm1 is required for hyperphosphorylation of Kin4 in vivo

Kin4 is subjected to cell cycle–dependent phosphorylation (D'Aquino et al., 2005). Thus, Elm1 could directly phosphorylate and regulate Kin4. To investigate the phosphorylation profile of Kin4 in *elm1Δ* cells, we analyzed Kin4-6HA from cells treated with nocodazole. This treatment increases the proportion of Kin4-6HA with the slow-migrating hyperphosphorylated forms (D'Aquino et al., 2005). In this experiment, cells were arrested in the G1 phase and then released in nocodazole-containing medium until metaphase arrest (Fig. 5 A). Although both wild-type and *rts1Δ* cells accumulated hyperphosphorylated Kin4-6HA as the cell cycle arrested (Fig. 5 A), hyperphosphorylation of Kin4-6HA was not observed in cells lacking *ELM1* (Fig. 5 A). The deletion of *ELM1* in *rts1Δ* cells also reduced the prominence of hyperphosphorylated Kin4-6HA bands, which suggests that increased Kin4 phosphorylation in *rts1Δ* cells also depends on Elm1 (Fig. S1 A). Kin4 hyperphosphorylation was also dependent on Elm1 in *kar9Δ act5-ts-deg* cells, which arrest with misaligned spindles in response to SPOC activation (Fig. S1 B; Hu et al., 2001; Maekawa et al., 2007). We conclude that Elm1 regulates the phosphorylation status of Kin4 in vivo.

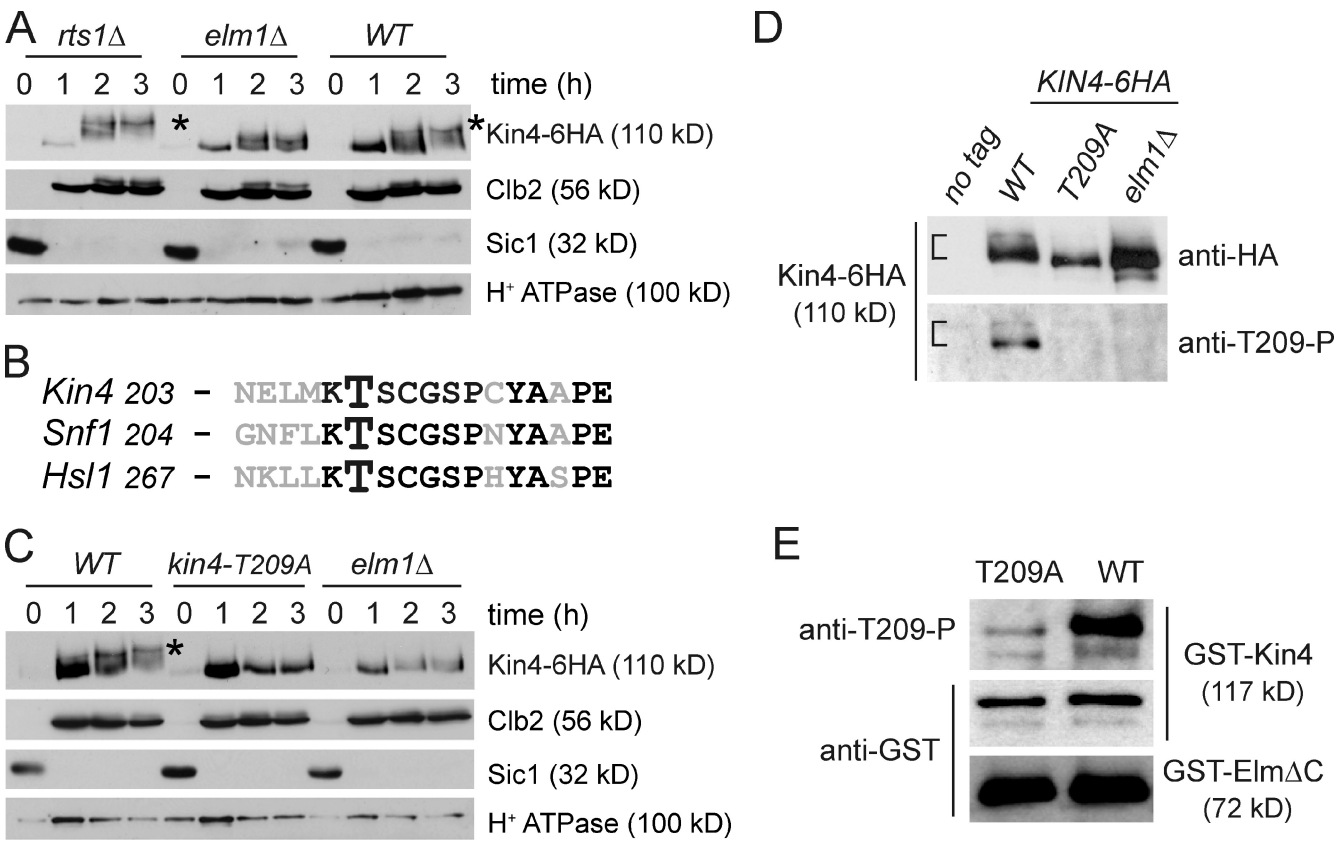

Figure 5. **Elm1 phosphorylates Kin4 at threonine 209.** (A) Indicated cells types were arrested in the G1 phase by α-factor (t_0) and released in nocodazole-containing medium. Samples were taken every hour and probed for Kin4-6HA, Clb2, and Sic1 by immunoblotting. H+ATPase served as loading control. (B) Sequence alignment of Kin4, Snf1, and Hsl1 activation loops. Identical residues are shown in black. The conserved threonine residue is enlarged. (C) α-Factor–arrested cells were released in nocodazole-containing medium. Samples were collected every hour and tested by immunoblotting as in A. (D) Cycling cultures of strains carrying *KIN4* (no tag), *KIN4-6HA* (WT), *kin4-T209A-6HA* (T209A), and *KIN4-6HA elm1Δ* were subjected to immunoprecipitation using anti-HA beads. Samples were probed with anti-HA and anti–T209-P antibodies by immunoblotting. The brackets depict the slower- and faster-migrating Kin4 forms. (E) In vitro phosphorylated GST-Kin4 and GST-Kin4-T209A by GST-Elm1ΔC were probed with anti-T209-P and anti-GST antibodies. Asterisks in A and C indicate hyperphosphorylated forms of Kin4.

We also analyzed the mobility shift of the Kin4-6HA band in synchronized cell cultures that had not been treated with nocodazole. In wild-type cells, the appearance of the slow-migrating forms of Kin4-6HA coincided with two markers of mitotic exit: Clb2 degradation and the accumulation of Sic1 (D'Aquino et al., 2005). In contrast, synchronized e*lm1Δ* cells failed to accumulate hyperphosphorylated forms of Kin4-6HA as they transitioned though the cell cycle. In *rts1Δ* cells, Kin4-6HA remained hyperphosphorylated throughout the cell cycle, as described previously (Fig. S1 C; Chan and Amon, 2009). Collectively, the data show that hyperphosphorylation of Kin4 depends on Elm1 activity.

Elm1 directly phosphorylates Kin4

Elm1 phosphorylates a threonine residue in the activation loop of Snf1 and Hsl1 kinases and thereby increases their kinase activities (Hong et al., 2003; Sutherland et al., 2003; Szkotnicki et al., 2008). The activation loop is a stretch of 10–15 amino acids that lies close to the catalytic domain of particular kinases (Hanks and Hunter, 1995; Adams, 2003). The activation loop region of Kin4 is highly reminiscent of those of Hsl1 and Snf1 (Figs. 5 B and S2), and the threonine, which is phosphorylated in both Hsl1 and Snf1 by Elm1, is also conserved in Kin4 (T209; Figs. 5 B and S2). Importantly, it has previously been shown that Kin4-T209A exhibits no kinase activity (Fig. 4 C; D'Aquino et al., 2005; Maekawa et al., 2007).

Together, these data would be consistent with a model in which Elm1 regulates Kin4 through phosphorylation of T209. To test this model, we asked whether Kin4-T209A is hyperphosphorylated in vivo. *kin4-T209A* cells failed to accumulate hyperphosphorylated forms of Kin4 upon nocodazole treatment (Fig. 5 C). Thus, T209 could be a putative phosphorylation site for Elm1. To test this further, we generated a phospho-specific polyclonal antibody that recognized phosphorylated, but not unphosphorylated, T209 (anti–T209-P). The specificity of the affinity purified anti–T209-P antibody for phosphorylated Kin4 was demonstrated by its ability to recognize Kin4 but not Kin4-T209A immunoprecipitated from yeast cells (Fig. 5 D). Importantly, the anti–T209-P antibodies failed to recognize Kin4 immunoprecipitated from *elm1Δ* cells (Fig. 5 D). The anti–T209-P antibodies also recognized the faster-migrating hypophosphorylated form of Kin4 in wild-type cells, which indicates that this form is already phosphorylated at T209 (Fig. 5 D, WT). Together, T209 of Kin4 is phosphorylated in an Elm1-dependent manner in vivo.

To test whether Elm1 directly phosphorylates T209 of Kin4 in vitro, we used the C-terminally truncated Elm1 (Elm1ΔC), which has elevated kinase activity (Sutherland et al., 2003). GST-Elm1ΔC was purified from yeast and incubated with bacterially expressed GST-Kin4 and GST-Kin4-T209A proteins. After incubation with GST-Elm1ΔC, the anti–T209-P antibody predominantly recognized GST-Kin4 but not GST-Kin4-T209A (Fig. 5 E). GST-Elm1ΔC also phosphorylated an N-terminal truncated Kin4 (Kin4-N) at T209 (Fig. S3, A–C). Phosphorylation of Kin4-N was drastically reduced after mutation of T209 to alanine, indicating that the T209 is the major site being phosphorylated by Elm1 at the N-terminal domain of Kin4. However, we cannot exclude that Elm1 phosphorylates additional sites in the N-terminal domain of Kin4. Collectively, the data show that Elm1 directly phosphorylates Kin4 at T209.

In vitro kinase assays using radioactive ATP, however, revealed that GST-Elm1ΔC was able to phosphorylate both bacterially expressed full-length GST-Kin4 and GST-Kin4-T209A (Fig. 6 A, lanes 2 and 3). Phosphorylation was caused by GST-Elm1ΔC, as no phosphorylation was observed when GST-Elm1ΔC kinase dead was used (GST-Elm1ΔC-KD; Fig. 6 A, lanes 5 and 6). Thus, Elm1 phosphorylates further sites in Kin4 in addition to T209.

In contrast to full length and Kin4-N, a bacterially expressed C-terminal construct of Kin4 (6His-Kin4-C; Fig. S3 A) was more soluble and could be purified in larger amounts. Elm1 was able to phosphorylate Kin4-C in vitro (Fig. 6 B). Mass spectrometric analysis of 6His-Kin4-C phosphorylated by Elm1 revealed five phosphopeptides (Fig. S3 D). Although the precise identity of the serine or threonine phosphorylated in each peptide could not be determined, some of residues within these peptides have been detected in previous in vivo studies (Li et al., 2007; Smolka et al., 2007; Albuquerque et al., 2008; Holt et al., 2009; Breitkreutz et al., 2010). Thus, in addition to T209, Elm1 also phosphorylates additional sites at the C terminus of Kin4.

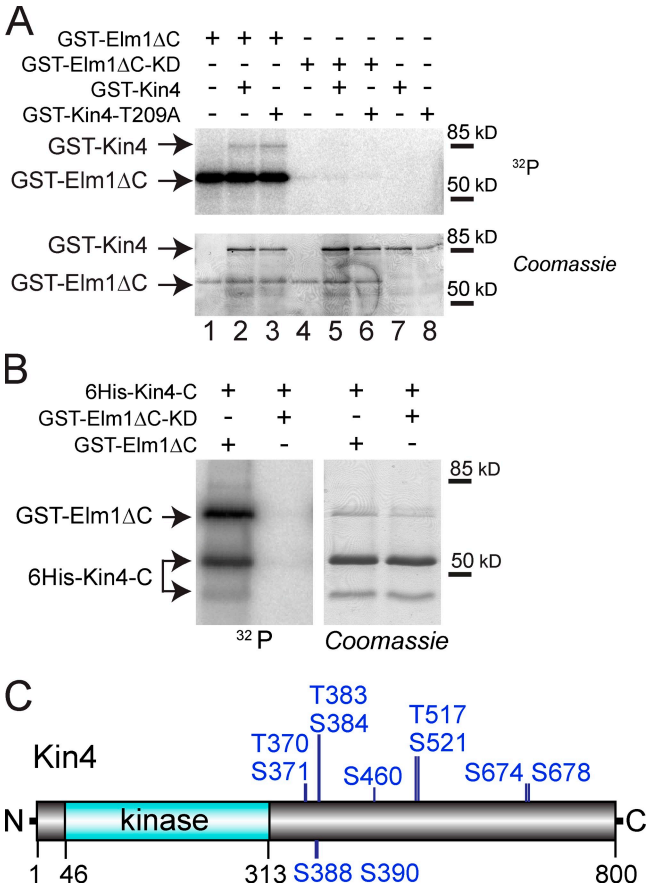

Figure 6. **Elm1 phosphorylates C-terminal Kin4.** In vitro kinase assays using purified GST-Elm1ΔC or GST-Elm1ΔC-KD and full-length GST-Kin4 and GST-Kin4-T209A (A) or the C-terminal domain of Kin4 (6His-Kin4-C; B). Autoradiographs and Coomassie-stained protein gels are shown. Note the autophosphorylation of Elm1. (C) Putative sites in 6His-Kin4-C phosphorylated by Elm1 in vitro, which were also detected in previously published in vivo studies (see text for details). Amino acid positions are indicated with numbers. N and C represent N and C termini, respectively. Domain positions shown are according to The UniProt Knowledgebase (UniProtKB).

kin4 mutants that cannot be phosphorylated by Elm1 are SPOC deficient

To study the function of Elm1 phosphorylation of Kin4 at position T209, we analyzed the phenotypes of cells with the nonphosphorylatable Kin4-T209A. As shown previously, the T209A substitution completely abolished Kin4 kinase activity in vivo and in vitro (Fig. 4 C). Moreover, cells carrying *kin4-T209A* were SPOC deficient (Fig. 7 A; D'Aquino et al., 2005; Maekawa et al., 2007). We also established that protein levels and Kin4 localization were not affected by the T209A (Figs. 7 B and S3 F). Together, these data strongly support the view that phosphorylation of T209 by Elm1 promotes Kin4 catalytic activity and thereby SPOC proficiency.

To study the functional consequences of Elm1-dependent phosphorylation at Kin4 C-terminal residues in vivo, we replaced the serines and threonines depicted in Fig. 6 C to alanine to mimic nonphosphorylatable Kin4 (*kin4-11A*). *kin4-11A* was integrated into the *KIN4* locus under its own promoter. Kin4-11A steady-state protein levels and localization were similar to those of wild-type Kin4, and the catalytic activity of Kin4-11A was comparable to Kin4 (Figs. 7 B and S3, F and G). However, the *kar9Δ kin4-11A* mutant accumulated more cells with broken spindles in the mother cell than *kar9Δ KIN4* cells (Fig. 7 A), which suggests that Elm1 phosphorylation of sites in the C terminus of Kin4 contributes to the SPOC function of Kin4. The SPOC deficiency of *kin4-11A* cells was not as severe as that of *kin4-T209A* cells (Fig. 7 A), which indicates that the predominant impact of Elm1 upon Kin4 function in the SPOC is mediated by the activating phosphorylation at position 209 of the activation loop.

Kin4 T209 phosphorylation peaks in metaphase

Next, we asked whether the phosphorylation of Kin4 at T209 by Elm1 is cell cycle regulated. Cells were arrested in G1, S phase, metaphase, or late anaphase, and Kin4-6HA was enriched by immunoprecipitation (Fig. 8 A). Monitoring the ratio of Kin4 phosphorylated at T209 to the total Kin4 amount showed that T209 phosphorylation peaked in metaphase (Fig. 8 A). We next

asked whether the levels of Kin4 T209 phosphorylation changed in response to microtubule defects. We arrested cells in metaphase by depletion of *CDC20* before adding nocodazole to the culture (Fig. 8 B). T209 phosphorylation of these metaphase-arrested cells was not significantly increased after the depolymerization of microtubules (Fig. 8 B). This indicates that phosphorylation of T209 does not increase in response to SPOC activation; rather, it suggests that Elm1 "licenses" Kin4 to be competent to act in the SPOC.

Sustained Elm1 bud neck localization is not primarily required to maintain Kin4 activity

To assess the importance of the bud neck localization of Kin4 and Elm1 for Kin4 control, we determined when in the cell cycle Elm1-GFP and Kin4-GFP reside at the bud neck. Elm1-GFP was recruited to the bud neck from G1/S and remained at this site until it disappeared 4 ± 2 min before the spindle collapsed (Fig. S4, A and C). We also analyzed cells arrested in late anaphase with misaligned spindles and found that Elm1-GFP persisted at the bud neck for the duration of this arrest (Fig. S4 D). Interestingly, Kin4-GFP was recruited to the bud neck 4 ± 3 min before spindle collapse (Fig. S4, B and C). This indicates that Kin4 and Elm1 co-resided, if at all, very transiently at the bud neck.

To clarify this point, we analyzed colocalization of Elm1 and Kin4 in the same cells. As the fluorescent signals from 3mCherry-tagged versions of Kin4 and Elm1 were too weak for time-lapse imaging, we performed population analysis of Kin4-GFP Elm1-3mCherry cultures without fixation. No colocalization of Kin4-GFP and Elm1-3mCherry could be detected in any anaphase cells (n = 200; Fig. 9 A). Furthermore, FRAP analysis of Elm1-GFP showed that the binding of Elm1-GFP to the bud neck was dynamic, with a half-life of 15 ± 6 s (Fig. S4 E). We therefore postulated that Elm1 and Kin4 do not need to interact at the bud neck for Elm1 to activate Kin4. This conclusion is consistent with the finding that Kin4 is already phosphorylated by Elm1 earlier in mitosis when Kin4 only associates with the mother cell cortex and not the bud neck.

To further investigate whether Elm1 needs to be retained at the bud neck to regulate Kin4, we used cells overexpressing a nondegradable form of the mitotic cyclin Clb2 (*clb2ΔDB* cells; Surana et al., 1993). These cells enter mitosis without forming a bud if *clb2ΔDB* is overexpressed before bud formation (Amon et al., 1994). Accordingly, we overexpressed *clb2ΔDB* before or after bud formation and, at the same time, induced a metaphase arrest by adding nocodazole to the cultures (Fig. 9 B). Thus, we obtained two homogeneous populations of cells that were arrested in metaphase. In one population (named budded), 95% of the cells had bud necks (Fig. 9 B, lane 1), whereas in the other population, 92% of the cells (named nonbudded) lacked a bud neck (Fig. 9, lane 2). Elm1-GFP localized to the bud neck in budded cells, whereas its localization was in the cytoplasm of nonbudded cells (Fig. S4 F). The Kin4-specific kinase activity was not reduced in nonbudded cells in comparison to budded cells (Fig. 9 B, lanes 1 and 2). Furthermore, we established that Kin4 kinase activity and hyperphosphorylation in metaphase-arrested nonbudded cells was still dependent on Elm1 (Fig. 9 B, lane 3; and Fig. 9 C).

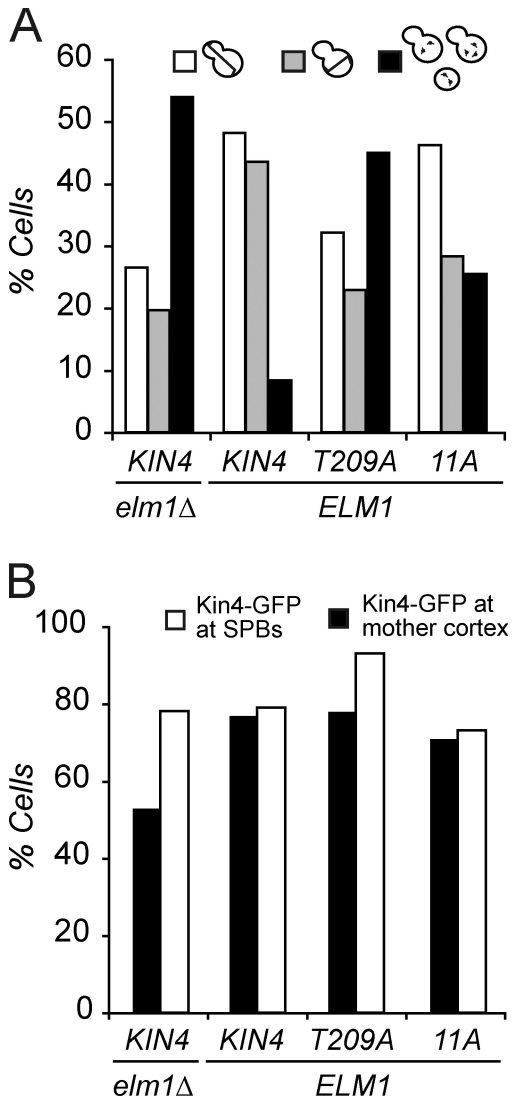

Figure 7. **Localization and SPOC activity of *KIN4* mutants.** (A) The indicated strains were incubated at 30°C for 3 h before fixation. The percentage of cells with normal (white bars), misaligned (gray bars), and broken spindles in one cell body (black bars, SPOC-deficient cells) are indicated. (B) Kin4-GFP localization was scored for the indicated strains. The graphs in A and B show one representative experiment out of three; 100–150 cells were counted per sample.

These data indicate that the maintenance of Elm1 at the bud neck is not an absolute prerequisite for Elm1-dependent Kin4 activation. Similar results were obtained for the septin-defective *cdc12-6* mutant (Barral et al., 2000), which did not form a functional bud neck and mislocalized Elm1 at the restrictive temperature (Figs. 9 D and S4 G).

Discussion

Here, we show that the bud neck–associated kinase Elm1 is essential to promote Kin4 catalytic activity. Our study uncovers a novel function for Elm1 in the regulation of Kin4 activation and SPOC signaling alongside the established roles for Elm1 in septin organization, bud morphogenesis, and cell cycle progression.

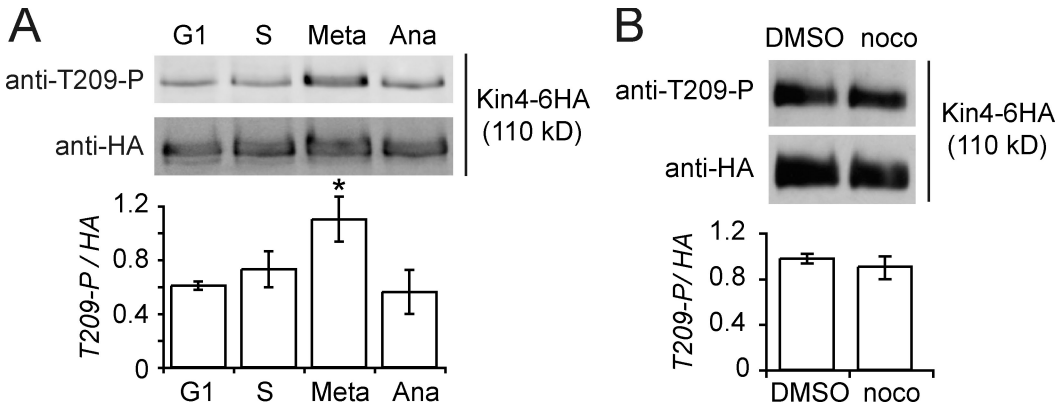

Figure 8. **T209 phosphorylation increases during metaphase independently of SPOC activation.** (A) Cells were arrested at G1 phase, S phase, metaphase (meta), and late anaphase (ana) by α-factor, hydroxyurea, Gal1-*CDC20* depletion, and *clb2ΔDB* overexpression, respectively. Kin4-6HA was immunoprecipitated from cell lysates and probed with anti-HA and anti–T209-P antibodies. Quantifications show the ratio of anti–T209-P to anti-HA signals. The graph represents the mean of five independent experiments. Error bars show the standard deviation. The asterisk indicates the group significantly different from the others ($P < 0.05$, *t* test). (B) *KIN4-6HA* Gal1-*CDC20* cells arrested in metaphase by Cdc20 depletion were treated with DMSO or nocodazole. Samples were analyzed and quantified as in A. The graph represents the mean of three independent experiments.

A genetic screen identifies *ELM1* as a positive regulator of Kin4

We identified the kinase *ELM1*, *RTS1*, and additional genes (unpublished data) in a genetic screening designed to isolate positive regulators of Kin4. Genetic analysis established that the role of Elm1 in regulating Kin4 was independent of Elm1 regulation of the established Elm1 effectors such as Gin4, Hsl1, and Snf1. Instead, we demonstrate that Elm1 is required for Kin4 activity. In *elm1Δ* cells, the specific kinase activity of immunoprecipitated Kin4 was drastically reduced and resembled the activity levels detected in immunoprecipitates from the inactive *kin4-T209A* mutant (Fig. 4). A complete lack of Kin4-specific kinase activity was also observed when Kin4 was enriched from *elm1Δ* cells upon SPOC activation. Consistently, *elm1Δ* cells were SPOC deficient and phenocopied *kin4Δ* cells.

How does Elm1 regulate Kin4?

Our data strongly support the view that Elm1 directly phosphorylates Kin4 independently of Rts1 function (Fig. 10). Purified Elm1 phosphorylated Kin4 in vitro and deletion of *ELM1* abolished Kin4 hyperphosphorylation in the presence or absence of *RTS1* in vivo. Interestingly, Kin4 hyperphosphorylation was lost in cells expressing a kinase-dead mutant of *KIN4* (Fig. 5). This suggested that Kin4 kinase activity might be required to promote Kin4 hyperphosphorylation either by autophosphorylation or in a positive feedback loop together with Elm1 or other kinases (Fig. 10). So far, we have been unable to detect Kin4 autophosphorylation in vitro. However, we cannot exclude the possibility that Kin4 might be subjected to autophosphorylation events that are dependent on a particular cellular context.

It is well established that Elm1 acts as an activating kinase for Snf1 and Hsl1 through phosphorylation of a conserved threonine in the activation loop (Hong et al., 2003; Sutherland et al., 2003; Szkotnicki et al., 2008). The activation loops of Snf1 and Hsl1 exhibit high sequence homology between amino acids 208 and 214 of Kin4. Using phospho-specific antibodies, we showed that Kin4 is phosphorylated at the conserved threonine 209 in an Elm1-dependent manner both in vivo and in vitro. This suggests that Elm1 directly regulates the activity of Kin4 kinase by modifying T209. Consistently, the phosphoinhibitory *kin4-T209A* mutation completely inhibited Kin4 catalytic activity, even in the presence of Elm1.

The molecular mechanism by which phosphorylation of T209 influences Kin4 catalytic function is currently unclear. Structural studies of kinases regulated by activation loop phosphorylation have implied that the loop might function as a "sensitive switch" that controls substrate binding triggered by phosphorylation-dependent conformational changes (Adams, 2003). It will be interesting to investigate whether Elm1-dependent phosphorylation controls Kin4 accordingly.

Elm1 phosphorylated additional residues in the C terminus of Kin4, and phosphoinhibitory mutations in these residues (*kin4-11A*) affected the SPOC function of Kin4 without decreasing the specific Kin4 kinase activity (Figs. 7 and S3 F). We suggest that phosphorylation of the C terminus of Kin4 might also facilitate Kin4 function in SPOC by a mechanism that is distinct from that governing T209 phosphorylation. At present it is unclear how C-terminal phosphorylation of Kin4 by Elm1 influences the SPOC in a molecular way. Although we did not observe any significant difference in the steady-state levels of Kin4-11A-GFP at the SPBs and cortex in comparison to Kin4-GFP, it is still possible that phosphorylation of the C-terminal domain of Kin4 by Elm1 might influence the binding dynamics of Kin4 to both subcellular structures, which in turn might influence the ability of Kin4 to function in SPOC.

Does Kin4 T209 phosphorylation fluctuate during the cell cycle?

We observed an increase in Kin4 T209 phosphorylation in cells arrested in metaphase (without SPOC activation) over other phases of the cell cycle. Interestingly, no significant difference in T209 phosphorylation was observed in metaphase-arrested cells before or after SPOC activation, which suggests that T209 phosphorylation is not regulated by the triggering of the SPOC. Consistently, it has been established that the specific kinase activity of Kin4 is high in metaphase irrespective of SPOC activation by

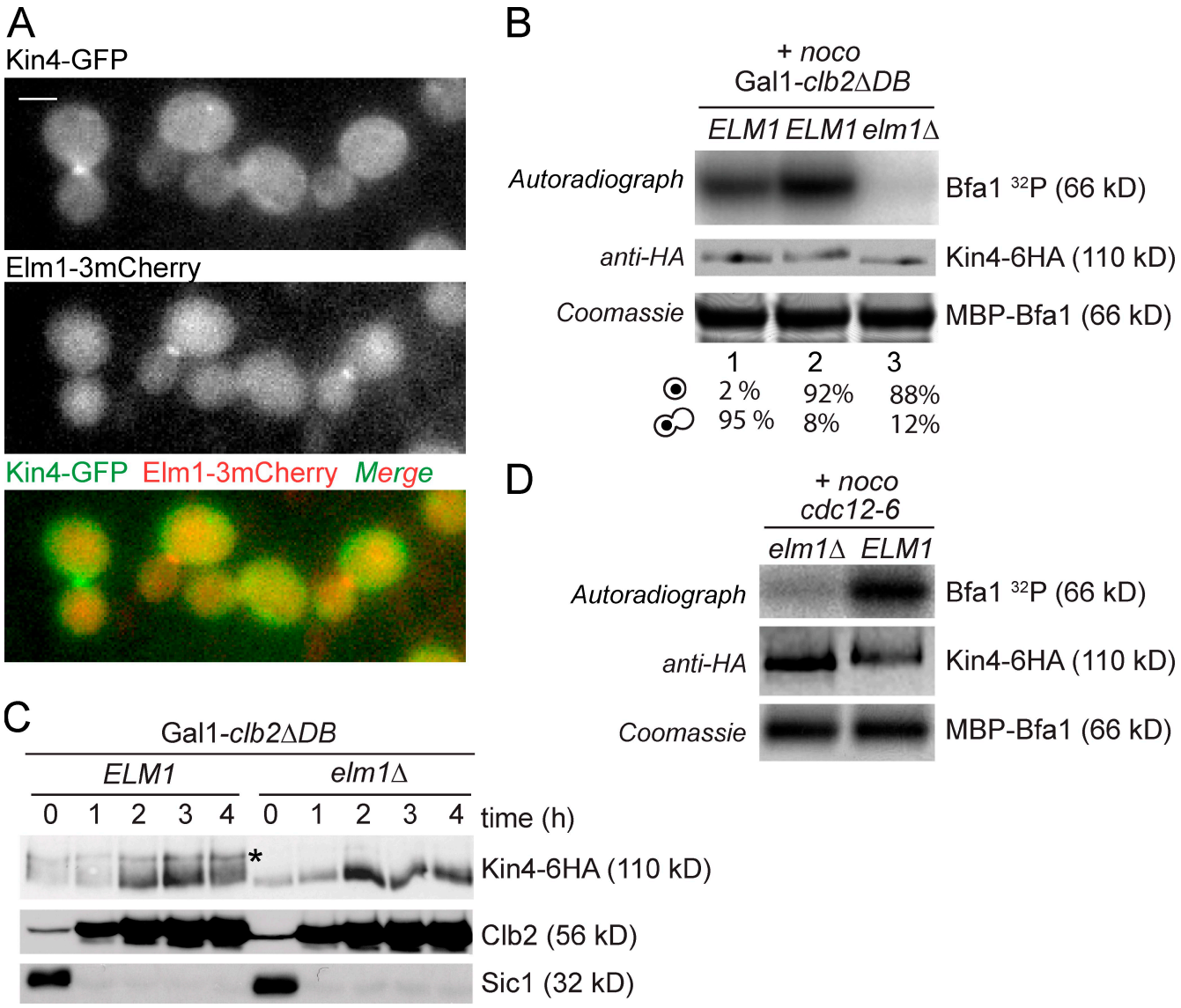

Figure 9. **Bud neck localization of Elm1 is not necessary for Kin4 activity.** (A) Still images of live *KIN4-GFP ELM1-3mCherry* cells. Bars, 3 µm. (B) Radioactive kinase assay of immunoprecipitated Kin4-6HA from Gal1-*clb2ΔDB*–overexpressing cells arrested with nocodazole with a bud neck (lane 1) and without a bud neck (lanes 2 and 3). The percentages of budded and nonbudded cells are indicated. See Materials and methods for details. (C) Both Gal1-*clb2ΔDB* and Gal1-*clb2ΔDB elm1Δ* cells were arrested with α-factor (G1-phase, t_0) and forced to enter mitosis without bud formation upon *clb2ΔDB* overexpression in the presence of nocodazole. Samples were taken every hour and analyzed by immunoblotting. The asterisk marks Kin4-hyperphosphorylated forms. (D) *cdc12-6* and *cdc12-6 elm1Δ* cells were arrested at 23°C with α-factor and released at 37°C in nocodazole-containing medium. In vitro kinase assays were performed using immunoprecipitated Kin4-6HA (anti-HA blot) and MBP-Bfa1 (Coomassie). Incorporation of the ^{32}P isotope in MBP-Bfa1 was measured by autoradiography.

microtubule depolymerization (D'Aquino et al., 2005). We favor the hypothesis that Elm1 phosphorylates Kin4 at threonine 209 to "license" Kin4 to operate in the SPOC irrespectively of whether a SPOC response has actually been triggered or not. Thus, Elm1 phosphorylation sets the stage for SPOC function in mitosis.

Role of Elm1 bud neck localization in SPOC

The integrity of the bud neck region has been proposed to have an important role in maintaining the SPOC arrest (Adames et al., 2001; Castillon et al., 2003; Moore et al., 2009). It is therefore tempting to speculate that Elm1 might provide the molecular link between bud neck integrity and sustained SPOC activity. Our data indicate that Elm1 and Kin4 do not colocalize at the bud neck. FRAP analysis revealed that Elm1 binds to the neck region in a dynamic manner, leaving one to ask whether Elm1 activates Kin4 locally or globally. Moreover, in cells progressing from G1 into a metaphase block without forming a bud neck, Elm1 stayed in the cytoplasm, and yet Kin4 kinase activity was not decreased with respect to metaphase-arrested cells that contained a bud neck and correctly localized Elm1 (Fig. 9 B). Thus, our data clearly indicate that a functional bud neck is not essential for the activation of Kin4 by Elm1. However, we cannot exclude the possibility that the bud neck might have a subtle influence upon the regulation of Kin4 by Elm1, for example through phosphorylation of sites in the C-terminal region of Kin4.

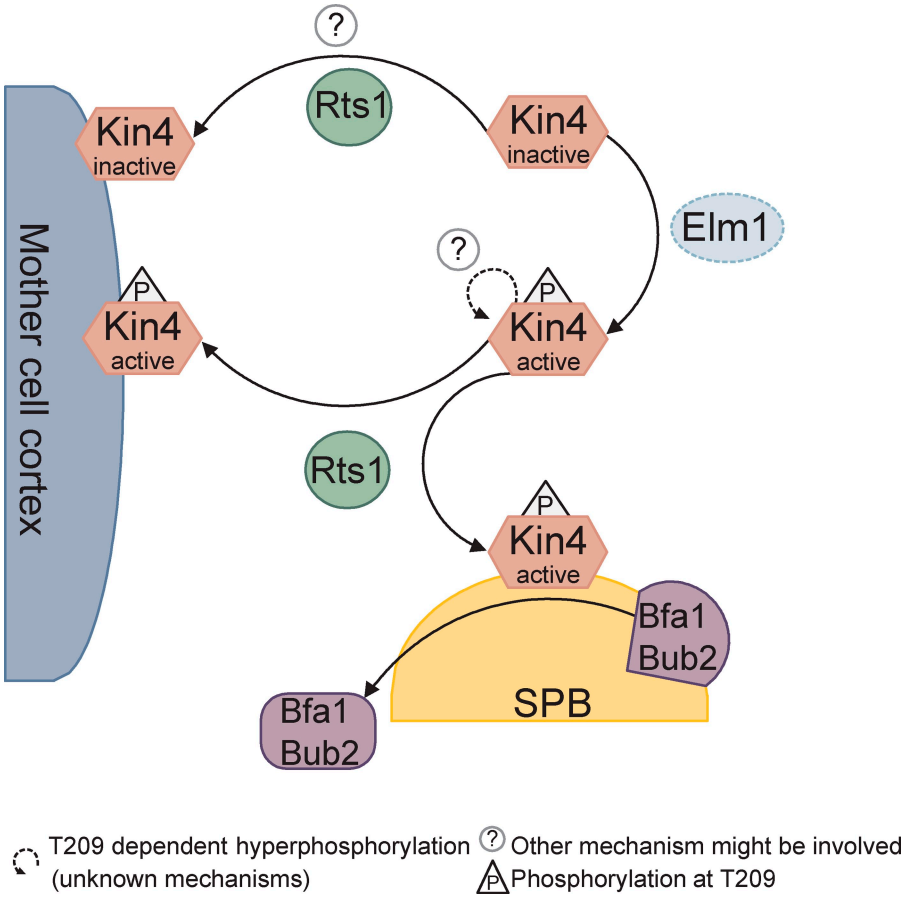

Figure 10. **Model depicting the mechanisms by which Elm1 and Rts1 regulate Kin4.** Elm1 phosphorylates Kin4 at threonine 209. This step is essential for Kin4 catalytic activity and subsequent hyperphosphorylation, which might require Kin4 kinase activity. Rts1 regulates Kin4 localization to the cortex and SPB (Chan and Amon, 2009; this study) by an unknown mechanism.

We observed that Elm1 stayed localized at the bud neck in cells arrested in late anaphase with misaligned spindles (Fig. S4 D). This suggests that Elm1 remains active in SPOC-arrested cells because Elm1 kinase activity was found to be necessary for its own association with the bud neck (Thomas et al., 2003). This might raise the question of whether SPOC directly inhibits Elm1 dissociation from the bud neck. However, the observation that cells arrested in late anaphase with correctly aligned spindles also retained Elm1 at the bud neck (unpublished data) argues against this hypothesis. Nevertheless, detailed analysis of Elm1 regulation will be necessary to shed light on this question.

Additional mechanisms that regulate Kin4

Cells lacking *RTS1* accumulated hyperphosphorylated and active Kin4 in an Elm1-dependent manner. However, the failure of SPOC function in *rts1Δ* cells most likely arises from the loss of Kin4 subcellular localization (Fig. 10; Chan and Amon, 2009). Thus, although Elm1 is crucial to promote Kin4 catalytic activity, the SPOC cannot function with active yet mislocalized Kin4. The identification of $PP2A^{Rts1}$ substrates and the demonstration that it is directly involved in Kin4 regulation will represent an important step in understanding SPOC regulation.

In yeast, Elm1, Sak1, and Tos3 kinases activate Snf1. Snf1 is the homologue of higher eukaryotic AMPK (Hong et al., 2003; Nath et al., 2003; Sutherland et al., 2003). Complementation experiments in yeast showed that deletion of *ELM1*, *SAK1*, and *TOS3* can be compensated by expression of mammalian LKB1, CaMKK, and TAK1 kinases, which are involved in AMPK activation (Hedbacker and Carlson, 2008; Williams and Brenman, 2008). This highlights the functional conservation of these kinases throughout evolution. Interestingly, AMPK functions in cell polarity, cell cycle, and metabolic control (Hardie, 2007). In yeast, Snf1 fulfills the role of AMPK in metabolic control. It is thus tempting to speculate that Kin4 might fulfill the roles executed by AMPK in coordinating polarity and mitotic control in yeast. Preliminary data suggest the existence of SPOC-like checkpoints in polarized cells of higher eukaryotes (O'Connell and Wang, 2000). It will be important to analyze the function of Kin4-like kinases in such control mechanisms.

Materials and methods

Yeast strains and plasmids

Yeast strains and plasmids used in this study are listed in the Table S1. All yeast strains are isogenic with S288C. Gene deletions and epitope tagging were performed using PCR-based methods (Knop et al., 1999; Janke et al., 2004). *GFP-TUB1* (Straight et al., 1997), Gal1-*CDC20* (Pereira and Schiebel, 2005), Met3-*CDC20* (Shirayama et al., 1999), and Gal1-*clb2ΔDB* (Surana et al., 1993) strains were constructed using integration plasmids. The red fluorescent eqFP (eqFP611; Wiedenmann et al., 2002) was fused to *SPC42* as an SPB marker. mCherry fused to *TUB1* was the red fluorescent monomeric Cherry, as described previously (Khmelinskii et al., 2007). Elm1 was fused to three tandem copies of mCherry (3mCherry; Maeder et al., 2007) using the plasmid pFA6a-3Cherry (a gift from M. Knop, European Molecular Biology Laboratory, Heidelberg, Germany).

Mutated genes on plasmids were integrated into the chromosomal *kin4ΔB* and *elm1ΔB* loci under the endogenous promoters. *kin4ΔB* and *elm1ΔB* loci were obtained by deleting the region between 100 bp downstream of START and 100 bp downstream of STOP codons of the corresponding genes, as described previously (Maekawa et al., 2007). All strains with *KAR9* deletion were kept with *KAR9* on a centromeric *URA3*-based plasmid and analyzed for phenotypes shortly after inducing plasmid loss on 5-fluoroorotic acid–containing plates.

Random UV mutagenesis screening

Overnight cultures of Gal1-*GFP-KIN4* Met25-*KIN4* cells plated on YPD agar plates (2,000 cells/plate) were immediately exposed to UV radiation of 9,000 μJ/cm^2 in a UV Crosslinker (Stratalinker). In total, 2.6 × 10^5 cells were mutagenized; 10% survived after irradiation. Survivors that could grow both on YP-Raf/Gal and SC-Met-Cys plates were selected as desired mutants. Kin4 expression levels were confirmed by immunoblotting. Strains with mutations in *BUB2* and *BFA1* were determined after complementation analysis by mating. The mutated genes responsible for growth rescue in other mutants were screened by complementation with a *LEU2*-based centromeric plasmid library (Cvrcková and Nasmyth, 1993).

Growth conditions

Basic yeast methods and growth media were as described previously (Sherman, 1991). Yeast strains were grown in yeast peptone dextrose medium with extra 0.1 mg/l adenine (YPAD) at 30°C unless otherwise specified. Temperature-sensitive strains (*cdc12-6* and *act5-ts-deg kar9Δ*) were grown at 23°C and shifted to 37°C for inspection of the phenotypes. For live-cell imaging, yeast cultures were grown in filter-sterilized synthetic complete medium. To induce the Gal1 promoter, 2% galactose was added to cells growing in medium containing 3% raffinose. For suppression of Gal1 promoter, 2% glucose was added to the media. Depletion of Met3 promoter was achieved by adding 2 mM methionine and 2 mM cysteine to the early log phase culture lacking methionine and cysteine.

Cell culture synchronizations

For synchronization of cells in the G1 phase, 10 μg/ml of synthetic α-factor (Sigma-Aldrich) was added to cultures in the early log phase (5 × 10^6 cells/ml) and incubated for ∼2.5 h until >95% of the cells formed mating projections. To arrest the cells with nocodazole, 15 μg/ml nocodazole (Sigma-Aldrich) was added to the culture media and incubated 2–4 h until >90% of the cells arrested with large buds and one DNA-stained region (DAPI staining). S phase arrest was induced by adding 200 μM hydroxyurea (Sigma-Aldrich) to log phase cultures and further incubating for 2 h. To provide late anaphase arrest, 2% galactose was added to the log phase culture of Gal1-*clb2ΔDB* cells grown in YP-Raf medium. Gal1-*CDC20* cells grown in raffinose/galactose media were arrested in metaphase by adding 2% glucose into the medium.

Experiments in Fig. 9 (B and C), were performed as follows: Gal1-*clb2ΔDB* cells were arrested at G1 phase with α-factor in raffinose medium. To obtain cell cycle progression without bud formation (nonbudded cells), galactose was added to the cultures immediately after release from the G1 phase block to provide Gal1-*clb2ΔDB* induction. To obtain budded cells, G1 phase blocked cells were allowed to grow first in raffinose media until >90% of the population formed small buds, and only then galactose was added to induce Gal1-*clb2ΔDB* overexpression. In both cases, nocodazole was added to the cultures after release of the G1 phase block and cells were analyzed after 2–3 h of nocodazole addition.

Fluorescence microscopy

Time-lapse and FRAP experiments were performed on glass-bottom dishes (MatTek) using 6% concanavalin A-Type IV (Sigma-Aldrich) for cell adhesion. Images were acquired at 30°C using a wide-field fluorescence imaging system (DeltaVision RT; Applied Precision) equipped with a 100×/1.40 NA UPLS Apochromat UIS2 oil immersion objective lens, a charge-coupled device camera (CoolSNAP HQ/ICX285; Photometrics), a quantifiable laser module, and SoftWoRx software (Applied Precision). Nineteen z stacks of 0.2 μm thickness were taken for Kin4-GFP (3-min intervals) and Elm1-GFP (every minute). For GFP-tubulin images, 12 z stacks of 0.3 μm thickness were taken every minute. FRAP of Elm1-GFP was performed by bleaching 80–100% of the Elm1-GFP at the bud neck with two laser (20 mW, 488 nm laser) iterations of 0.01 s duration (50% intensity) each, and by acquiring single plane pre- and postbleach images. The mean signal intensity at the entire bud neck region was quantified using ImageJ (National Institutes of Health) software, corrected for acquisition bleaching, and normalized as described in Caydasi and Pereira (2009). FRAP recovery curves were fitted to a single exponential curve (y = yo + Ae − bx) using IgorPro 6.02 (WaveMetrics) software. Half recovery times were calculated as –ln0.5b. Time-lapse images of Elm1-GFP and Kin4-GFP shown in Fig. S4 (A and B) were deconvolved and z-projected using SoftWoRx. In other figures, z stacks were projected without deconvolution using ImageJ software.

Still images were acquired using a microscope (Axiophot; Carl Zeiss, Inc.) equipped with a 100× 1.45 NA Plan-Fluor oil immersion objective lens (Carl Zeiss, Inc.), charge-coupled device camera (Cascade 1K; Photometrics), and MetaMorph software (Universal Imaging Corp.). Kin4-GFP and Elm1-GFP images were taken without cell fixation. For budding index counting, cells were fixed with 70% ethanol and resuspended in PBS containing 1 μg/ml DAPI (Sigma-Aldrich). The size of the buds and the distribution of DNA-stained regions were counted for 100–150 cells per time point. For visualization of GFP-tubulin, cells were fixed using 4% paraformaldehyde for 10 min at room temperature as described previously (Pereira et al., 2001).

Images were processed in ImageJ, Photoshop CS3 (Adobe), and Illustrator CS3 (Adobe). No manipulations were performed other than brightness, contrast, and color balance adjustments.

SPOC proficiency analysis

For population analysis of SPOC proficiency, *GFP-TUB1 kar9Δ* cells grown at 23°C were shifted to 30°C and incubated for 3 h. Cells were fixed by 4% paraformaldehyde and still images were taken to visualize GFP-tubulin. Cells with normal and misaligned intact anaphase spindles and cells with broken spindles in one cell body were counted.

Time-lapse videos of *GFP-TUB1 kar9Δ* cells were taken for 1–1.5 h with 1-min time intervals at 30°C. Anaphase duration was determined as the time from the start of spindle elongation until spindle breakdown (Straight et al., 1997).

Protein methods

Yeast protein extracts and Western blotting were performed as described previously (Janke et al., 2004). In brief, cell pellets were collected by centrifugation and resuspended in 1 ml of 250 mM NaOH, 7.5% TCA, and incubated on ice for 15 min. Samples were centrifuged at 10,000 *g* for 20 min at 4°C. Precipitated proteins were resuspended in HU-DTT (200 mM Tris-HCl, pH 6.8, 8 M urea, 5% SDS, 0.1 mM EDTA, 0.005% bromophenol blue, and 15 mg/ml DTT). Samples were heated up for 15 min at 65°C before loading on SDS-PAGE gels. Coomassie Brilliant Blue G-250 was used to stain protein gels. Antibodies were rabbit anti-GFP, mouse anti-GST, and rabbit anti-Bfa1 (gifts from E. Schiebel, Center for Molecular Biology, Heidelberg, Germany); mouse anti-tubulin (TAT1; Sigma-Aldrich), mouse anti-HA (12CA5; Sigma-Aldrich), rabbit anti-Clb2, and guinea pig anti-Sic1 (Maekawa et al., 2007); and mouse anti-H$^+$ATPase (Invitrogen) and mouse anti-His (GE Healthcare). Secondary antibodies used were goat anti–mouse, goat anti–rabbit, and goat anti–guinea pig IgGs coupled to horseradish peroxidase (Jackson ImmunoResearch Laboratories, Inc.). The anti–Kin4-T209-P antibody was raised in rabbits using the peptide DNELMK(p)TSCGSPC, in which (p) denotes the phosphorylated threonine (Peptide Specialty Laboratories GmbH). Antibodies were purified from the pre-absorbed sera by affinity purification using the immobilized phosphopeptide.

Amino acid sequence alignment

The kinase domains (according to UniProt Knowledgebase [UniProtKB]) of Hsl1, Snf1, and Kin4 were aligned using the JalView software (Waterhouse et al., 2009). Conserved domains are colored. Subdomain positions are determined according to the homology to Snf1 subdomains predicted by Hanks and Hunter (1995).

Recombinant protein purifications

MBP-Bfa1 from *Escherichia coli* were purified as described previously (Maekawa et al., 2007; Geymonat et al., 2009). GST-Kin4, 6His-Kin4-C, and 6His-Kin4-N were induced in *E. coli* BL21(DE3) at 23°C and purified according to the manufacturer's instructions (GE Healthcare and EMD). Buffer exchange of 6His fusion proteins was performed using PD MiniTrap G-25 sephadex columns (GE Healthcare). GST-Elm1ΔC and GST-Elm1ΔC-KD were purified from yeast cultures according to the method described by Geymonat et al. (2009).

Immunoprecipitation experiments

Pellets from a 100-ml yeast culture (10^7 cells/ml) were lysed in a FastPrep FP120 Cell Disturber (MP Biomedicals) using acid-washed glass beads (Sigma-Aldrich). Lysis buffer contained 50 mM Tris-HCl, pH 7.5, 150 mM NaCl, 10% glycerol, 1 mM EDTA, 1 mM DTT, 350 μg/ml benzamidine, 100 mM β-glycerophosphate, 50 mM NaF, 5 mM $NaVO_3$, and complete

EDTA-free protease inhibitor cocktail (Roche). Cell lysates were incubated with 1% nonyphenylpolyethylane glycol (NP-40) for 15 min, and total extracts were clarified by centrifugation at 10,000 g for 10 min. Kin4-6HA was immunoprecipitated from total extracts using anti-HA coupled protein A–Sepharose beads (GE Healthcare).

In vitro kinase assay

In vitro kinase assays of immunoprecipitated Kin4-6HA were performed in a kinase reaction buffer containing 20 mM Hepes, pH 7.4, 0.5 mM EDTA, 0.5 mM DTT, 5 mM $MgCl_2$, 0.05 µM ATP, and MBP-Bfa1 purified from *E. coli*. Reactions were held for 30 min at 30°C. Elm1 kinase assays were as described previously (Koehler and Myers, 1997). In brief, GST-Elm1ΔC kinase reactions contained 40 mM Tris-HCl, pH 7.5, 1 mM DTT, 10 mM $MgCl_2$, 5 mM NaF, 0.05 µM ATP, and bacterially purified Kin4 as a substrate. 5 µCi γ-[^{32}P]ATP (0.05 nM) was used per radioactive kinase reaction. Radioactivity was detected using a Bas 1800 II imaging system (Fujifilm).

Quantification of protein bands

The signal intensities of protein bands on protein gels (SDS-PAGE) stained with Coomassie, immunoblots, and autoradiographs were measured using the ImageJ software. Signal intensities were corrected against the gel background signal. Specific Kin4 kinase activity was calculated by dividing the amount of ^{32}P incorporated in MBP-Bfa1 to the relative amounts of immunoprecipitated Kin4-6HA, and MBP-Bfa1. The ratio of T209-P/Kin4-6HA in each individual sample was calculated as the percentage within each experimental set. After averaging independent experiments, the highest value was set to 1. The mean of Kin4 kinase activity was calculated in the same way.

Online supplemental material

Fig. S1 shows the mobility shift of the Kin4 in synchronized cell cultures. Fig. S2 presents the alignment of Hsl1, Snf1, and Kin4 kinase domains. Fig. S3 shows in vitro phosphorylation of Kin4-N terminal by Elm1 and Bfa1 by Kin4-11A. Fig. S4 shows the localization of Elm1 and Kin4 at the bud neck. Table S1 presents the list of strains and plasmids used in this study. Online supplemental material is available at http://www.jcb.org/cgi/content/full/jcb.201006151/DC1.

We acknowledge Daniela Lazzarini, and Renate Voit for technical advise; Elmar Schiebel and Ingrid Grummt for sharing equipment; Martina Schnölzer, Duncan Smith, and Thomas Ruppert for mass spectrometry analysis; Elmar Schiebel, Iain Hagan, and Fouzia Ahmad for critically reading the manuscript; and people from the E. Schiebel and G.P. laboratories for comments and discussions.

The work of G. Pereira is supported by a Helmholtz association grant (HZ-NG-111) and a Marie Curie fellowship (MEXT-CT-2006-042544). A.K. Caydasi is funded by the HZ-NG-111 grant and by the German Cancer Research Center (DKFZ) international PhD Program. B. Kurtulmus is funded by the Marie Curie fellowship (MEXT-CT-2006-042544).

Submitted: 25 June 2010
Accepted: 19 August 2010

References

Adames, N.R., J.R. Oberle, and J.A. Cooper. 2001. The surveillance mechanism of the spindle position checkpoint in yeast. *J. Cell Biol.* 153:159–168. doi:10.1083/jcb.153.1.159

Adams, J.A. 2003. Activation loop phosphorylation and catalysis in protein kinases: is there functional evidence for the autoinhibitor model? *Biochemistry.* 42:601–607. doi:10.1021/bi020617o

Albuquerque, C.P., M.B. Smolka, S.H. Payne, V. Bafna, J. Eng, and H. Zhou. 2008. A multidimensional chromatography technology for in-depth phosphoproteome analysis. *Mol. Cell. Proteomics.* 7:1389–1396. doi:10.1074/mcp.M700468-MCP200

Amon, A., S. Irniger, and K. Nasmyth. 1994. Closing the cell cycle circle in yeast: G2 cyclin proteolysis initiated at mitosis persists until the activation of G1 cyclins in the next cycle. *Cell.* 77:1037–1050. doi:10.1016/0092-8674(94)90443-X

Asano, S., J.E. Park, L.R. Yu, M. Zhou, K. Sakchaisri, C.J. Park, Y.H. Kang, J. Thorner, T.D. Veenstra, and K.S. Lee. 2006. Direct phosphorylation and activation of a Nim1-related kinase Gin4 by Elm1 in budding yeast. *J. Biol. Chem.* 281:27090–27098. doi:10.1074/jbc.M601483200

Bardin, A.J., and A. Amon. 2001. Men and sin: what's the difference? *Nat. Rev. Mol. Cell Biol.* 2:815–826. doi:10.1038/35099020

Bardin, A.J., R. Visintin, and A. Amon. 2000. A mechanism for coupling exit from mitosis to partitioning of the nucleus. *Cell.* 102:21–31. doi:10.1016/S0092-8674(00)00007-6

Barral, Y., M. Parra, S. Bidlingmaier, and M. Snyder. 1999. Nim1-related kinases coordinate cell cycle progression with the organization of the peripheral cytoskeleton in yeast. *Genes Dev.* 13:176–187. doi:10.1101/gad.13.2.176

Barral, Y., V. Mermall, M.S. Mooseker, and M. Snyder. 2000. Compartmentalization of the cell cortex by septins is required for maintenance of cell polarity in yeast. *Mol. Cell.* 5:841–851. doi:10.1016/S1097-2765(00)80324-X

Blacketer, M.J., C.M. Koehler, S.G. Coats, A.M. Myers, and P. Madaule. 1993. Regulation of dimorphism in *Saccharomyces cerevisiae*: involvement of the novel protein kinase homolog Elm1p and protein phosphatase 2A. *Mol. Cell. Biol.* 13:5567–5581.

Bloecher, A., G.M. Venturi, and K. Tatchell. 2000. Anaphase spindle position is monitored by the BUB2 checkpoint. *Nat. Cell Biol.* 2:556–558. doi:10.1038/35019601

Bouquin, N., Y. Barral, R. Courbeyrette, M. Blondel, M. Snyder, and C. Mann. 2000. Regulation of cytokinesis by the Elm1 protein kinase in *Saccharomyces cerevisiae*. *J. Cell Sci.* 113:1435–1445.

Breitkreutz, A., H. Choi, J.R. Sharom, L. Boucher, V. Neduva, B. Larsen, Z.Y. Lin, B.J. Breitkreutz, C. Stark, G. Liu, et al. 2010. A global protein kinase and phosphatase interaction network in yeast. *Science.* 328:1043–1046. doi:10.1126/science.1176495

Casamayor, A., and M. Snyder. 2002. Bud-site selection and cell polarity in budding yeast. *Curr. Opin. Microbiol.* 5:179–186. doi:10.1016/S1369-5274(02)00300-4

Castillon, G.A., N.R. Adames, C.H. Rosello, H.S. Seidel, M.S. Longtine, J.A. Cooper, and R.A. Heil-Chapdelaine. 2003. Septins have a dual role in controlling mitotic exit in budding yeast. *Curr. Biol.* 13:654–658. doi:10.1016/S0960-9822(03)00247-1

Caydasi, A.K., and G. Pereira. 2009. Spindle alignment regulates the dynamic association of checkpoint proteins with yeast spindle pole bodies. *Dev. Cell.* 16:146–156. doi:10.1016/j.devcel.2008.10.013

Chan, L.Y., and A. Amon. 2009. The protein phosphatase 2A functions in the spindle position checkpoint by regulating the checkpoint kinase Kin4. *Genes Dev.* 23:1639–1649. doi:10.1101/gad.1804609

Cvrcková, F., and K. Nasmyth. 1993. Yeast G1 cyclins CLN1 and CLN2 and a GAP-like protein have a role in bud formation. *EMBO J.* 12:5277–5286.

D'Aquino, K.E., F. Monje-Casas, J. Paulson, V. Reiser, G.M. Charles, L. Lai, K.M. Shokat, and A. Amon. 2005. The protein kinase Kin4 inhibits exit from mitosis in response to spindle position defects. *Mol. Cell.* 19:223–234. doi:10.1016/j.molcel.2005.06.005

Donaldson, A.D., and J.V. Kilmartin. 1996. Spc42p: a phosphorylated component of the *S. cerevisiae* spindle pole body (SPD) with an essential function during SPB duplication. *J. Cell Biol.* 132:887–901. doi:10.1083/jcb.132.5.887

Edgington, N.P., M.J. Blacketer, T.A. Bierwagen, and A.M. Myers. 1999. Control of *Saccharomyces cerevisiae* filamentous growth by cyclin-dependent kinase Cdc28. *Mol. Cell. Biol.* 19:1369–1380.

Evangelista, C.C. Jr., A.M. Rodriguez Torres, M.P. Limbach, and R.S. Zitomer. 1996. Rox3 and Rts1 function in the global stress response pathway in baker's yeast. *Genetics.* 142:1083–1093.

Fraschini, R., M. Venturetti, E. Chiroli, and S. Piatti. 2008. The spindle position checkpoint: how to deal with spindle misalignment during asymmetric cell division in budding yeast. *Biochem. Soc. Trans.* 36:416–420. doi:10.1042/BST0360416

Geymonat, M., A. Spanos, S.J. Smith, E. Wheatley, K. Rittinger, L.H. Johnston, and S.G. Sedgwick. 2002. Control of mitotic exit in budding yeast. In vitro regulation of Tem1 GTPase by Bub2 and Bfa1. *J. Biol. Chem.* 277:28439–28445. doi:10.1074/jbc.M202540200

Geymonat, M., A. Spanos, P.A. Walker, L.H. Johnston, and S.G. Sedgwick. 2003. In vitro regulation of budding yeast Bfa1/Bub2 GAP activity by Cdc5. *J. Biol. Chem.* 278:14591–14594. doi:10.1074/jbc.C300059200

Geymonat, M., A. Spanos, and S. Sedgwick. 2009. Production of mitotic regulators using an autoselection system for protein expression in budding yeast. *Methods Mol. Biol.* 545:63–80. doi:10.1007/978-1-60327-993-2_4

Hanks, S.K., and T. Hunter. 1995. Protein kinases 6. The eukaryotic protein kinase superfamily: kinase (catalytic) domain structure and classification. *FASEB J.* 9:576–596.

Hardie, D.G. 2007. AMP-activated/SNF1 protein kinases: conserved guardians of cellular energy. *Nat. Rev. Mol. Cell Biol.* 8:774–785. doi:10.1038/nrm2249

Hedbacker, K., and M. Carlson. 2008. SNF1/AMPK pathways in yeast. *Front. Biosci.* 13:2408–2420. doi:10.2741/2854

Holt, L.J., B.B. Tuch, J. Villén, A.D. Johnson, S.P. Gygi, and D.O. Morgan. 2009. Global analysis of Cdk1 substrate phosphorylation sites provides insights into evolution. *Science.* 325:1682–1686. doi:10.1126/science.1172867

Hong, S.P., F.C. Leiper, A. Woods, D. Carling, and M. Carlson. 2003. Activation of yeast Snf1 and mammalian AMP-activated protein kinase by upstream kinases. *Proc. Natl. Acad. Sci. USA.* 100:8839–8843. doi:10.1073/pnas.1533136100

Hu, F., Y. Wang, D. Liu, Y. Li, J. Qin, and S.J. Elledge. 2001. Regulation of the Bub2/Bfa1 GAP complex by Cdc5 and cell cycle checkpoints. *Cell.* 107:655–665. doi:10.1016/S0092-8674(01)00580-3

Janke, C., M.M. Magiera, N. Rathfelder, C. Taxis, S. Reber, H. Maekawa, A. Moreno-Borchart, G. Doenges, E. Schwob, E. Schiebel, and M. Knop. 2004. A versatile toolbox for PCR-based tagging of yeast genes: new fluorescent proteins, more markers and promoter substitution cassettes. *Yeast.* 21:947–962. doi:10.1002/yea.1142

Khmelinskii, A., C. Lawrence, J. Roostalu, and E. Schiebel. 2007. Cdc14-regulated midzone assembly controls anaphase B. *J. Cell Biol.* 177:981–993. doi:10.1083/jcb.200702145

Knop, M., K. Siegers, G. Pereira, W. Zachariae, B. Winsor, K. Nasmyth, and E. Schiebel. 1999. Epitope tagging of yeast genes using a PCR-based strategy: more tags and improved practical routines. *Yeast.* 15(10B):963–972. doi:10.1002/(SICI)1097-0061(199907)15:10B<963::AID-YEA399>3.0.CO;2-W

Koehler, C.M., and A.M. Myers. 1997. Serine-threonine protein kinase activity of Elm1p, a regulator of morphologic differentiation in *Saccharomyces cerevisiae. FEBS Lett.* 408:109–114. doi:10.1016/S0014-5793(97)00401-8

Lew, D.J., and D.J. Burke. 2003. The spindle assembly and spindle position checkpoints. *Annu. Rev. Genet.* 37:251–282. doi:10.1146/annurev.genet.37.042203.120656

Lew, D.J., and S.I. Reed. 1995. A cell cycle checkpoint monitors cell morphogenesis in budding yeast. *J. Cell Biol.* 129:739–749. doi:10.1083/jcb.129.3.739

Li, X., S.A. Gerber, A.D. Rudner, S.A. Beausoleil, W. Haas, J. Villén, J.E. Elias, and S.P. Gygi. 2007. Large-scale phosphorylation analysis of alpha-factor-arrested *Saccharomyces cerevisiae. J. Proteome Res.* 6:1190–1197. doi:10.1021/pr060559j

Maeder, C.I., M.A. Hink, A. Kinkhabwala, R. Mayr, P.I. Bastiaens, and M. Knop. 2007. Spatial regulation of Fus3 MAP kinase activity through a reaction-diffusion mechanism in yeast pheromone signalling. *Nat. Cell Biol.* 9:1319–1326. doi:10.1038/ncb1652

Maekawa, H., C. Priest, J. Lechner, G. Pereira, and E. Schiebel. 2007. The yeast centrosome translates the positional information of the anaphase spindle into a cell cycle signal. *J. Cell Biol.* 179:423–436. doi:10.1083/jcb.200705197

Manderson, E.N., M. Malleshaiah, and S.W. Michnick. 2008. A novel genetic screen implicates Elm1 in the inactivation of the yeast transcription factor SBF. *PLoS One.* 3:e1500. doi:10.1371/journal.pone.0001500

Miller, R.K., and M.D. Rose. 1998. Kar9p is a novel cortical protein required for cytoplasmic microtubule orientation in yeast. *J. Cell Biol.* 140:377–390. doi:10.1083/jcb.140.2.377

Molk, J.N., S.C. Schuyler, J.Y. Liu, J.G. Evans, E.D. Salmon, D. Pellman, and K. Bloom. 2004. The differential roles of budding yeast Tem1p, Cdc15p, and Bub2p protein dynamics in mitotic exit. *Mol. Biol. Cell.* 15:1519–1532. doi:10.1091/mbc.E03-09-0708

Monje-Casas, F., and A. Amon. 2009. Cell polarity determinants establish asymmetry in MEN signaling. *Dev. Cell.* 16:132–145. doi:10.1016/j.devcel.2008.11.002

Moore, J.K., V. Magidson, A. Khodjakov, and J.A. Cooper. 2009. The spindle position checkpoint requires positional feedback from cytoplasmic microtubules. *Curr. Biol.* 19:2026–2030. doi:10.1016/j.cub.2009.10.020

Mortensen, E.M., H. McDonald, J. Yates III, and D.R. Kellogg. 2002. Cell cycle-dependent assembly of a Gin4-septin complex. *Mol. Biol. Cell.* 13:2091–2105. doi:10.1091/mbc.01-10-0500

Nath, N., R.R. McCartney, and M.C. Schmidt. 2003. Yeast Pak1 kinase associates with and activates Snf1. *Mol. Cell. Biol.* 23:3909–3917. doi:10.1128/MCB.23.11.3909-3917.2003

O'Connell, C.B., and Y.L. Wang. 2000. Mammalian spindle orientation and position respond to changes in cell shape in a dynein-dependent fashion. *Mol. Biol. Cell.* 11:1765–1774.

Pereira, G., and E. Schiebel. 2001. The role of the yeast spindle pole body and the mammalian centrosome in regulating late mitotic events. *Curr. Opin. Cell Biol.* 13:762–769. doi:10.1016/S0955-0674(00)00281-7

Pereira, G., and E. Schiebel. 2005. Kin4 kinase delays mitotic exit in response to spindle alignment defects. *Mol. Cell.* 19:209–221. doi:10.1016/j.molcel.2005.05.030

Pereira, G., T. Höfken, J. Grindlay, C. Manson, and E. Schiebel. 2000. The Bub2p spindle checkpoint links nuclear migration with mitotic exit. *Mol. Cell.* 6:1–10. doi:10.1016/S1097-2765(00)00002-2

Pereira, G., T.U. Tanaka, K. Nasmyth, and E. Schiebel. 2001. Modes of spindle pole body inheritance and segregation of the Bfa1p-Bub2p checkpoint protein complex. *EMBO J.* 20:6359–6370. doi:10.1093/emboj/20.22.6359

Segal, M., and K. Bloom. 2001. Control of spindle polarity and orientation in *Saccharomyces cerevisiae. Trends Cell Biol.* 11:160–166. doi:10.1016/S0962-8924(01)01954-7

Sherman, F. 1991. Getting started with yeast. *Methods Enzymol.* 194:3–21. doi:10.1016/0076-6879(91)94004-V

Shirayama, M., W. Zachariae, R. Ciosk, and K. Nasmyth. 1998. The Polo-like kinase Cdc5p and the WD-repeat protein Cdc20p/fizzy are regulators and substrates of the anaphase promoting complex in *Saccharomyces cerevisiae. EMBO J.* 17:1336–1349. doi:10.1093/emboj/17.5.1336

Shirayama, M., A. Tóth, M. Gálová, and K. Nasmyth. 1999. APC(Cdc20) promotes exit from mitosis by destroying the anaphase inhibitor Pds1 and cyclin Clb5. *Nature.* 402:203–207. doi:10.1038/46080

Shu, Y., H. Yang, E. Hallberg, and R. Hallberg. 1997. Molecular genetic analysis of Rts1p, a B' regulatory subunit of *Saccharomyces cerevisiae* protein phosphatase 2A. *Mol. Cell. Biol.* 17:3242–3253.

Sia, R.A., H.A. Herald, and D.J. Lew. 1996. Cdc28 tyrosine phosphorylation and the morphogenesis checkpoint in budding yeast. *Mol. Biol. Cell.* 7:1657–1666.

Smolka, M.B., C.P. Albuquerque, S.H. Chen, and H. Zhou. 2007. Proteome-wide identification of in vivo targets of DNA damage checkpoint kinases. *Proc. Natl. Acad. Sci. USA.* 104:10364–10369. doi:10.1073/pnas.0701622104

Sreenivasan, A., and D. Kellogg. 1999. The elm1 kinase functions in a mitotic signaling network in budding yeast. *Mol. Cell. Biol.* 19:7983–7994.

Straight, A.F., W.F. Marshall, J.W. Sedat, and A.W. Murray. 1997. Mitosis in living budding yeast: anaphase A but no metaphase plate. *Science.* 277:574–578. doi:10.1126/science.277.5325.574

Surana, U., A. Amon, C. Dowzer, J. McGrew, B. Byers, and K. Nasmyth. 1993. Destruction of the CDC28/CLB mitotic kinase is not required for the metaphase to anaphase transition in budding yeast. *EMBO J.* 12:1969–1978.

Sutherland, C.M., S.A. Hawley, R.R. McCartney, A. Leech, M.J. Stark, M.C. Schmidt, and D.G. Hardie. 2003. Elm1p is one of three upstream kinases for the *Saccharomyces cerevisiae* SNF1 complex. *Curr. Biol.* 13:1299–1305. doi:10.1016/S0960-9822(03)00459-7

Szkotnicki, L., J.M. Crutchley, T.R. Zyla, E.S. Bardes, and D.J. Lew. 2008. The checkpoint kinase Hsl1p is activated by Elm1p-dependent phosphorylation. *Mol. Biol. Cell.* 19:4675–4686. doi:10.1091/mbc.E08-06-0663

Thomas, C.L., M.J. Blacketer, N.P. Edgington, and A.M. Myers. 2003. Assembly interdependence among the *S. cerevisiae* bud neck ring proteins Elm1p, Hsl1p and Cdc12p. *Yeast.* 20:813–826. doi:10.1002/yea.1003

Waterhouse, A.M., J.B. Procter, D.M. Martin, M. Clamp, and G.J. Barton. 2009. Jalview Version 2—a multiple sequence alignment editor and analysis workbench. *Bioinformatics.* 25:1189–1191. doi:10.1093/bioinformatics/btp033

Wiedenmann, J., A. Schenk, C. Röcker, A. Girod, K.D. Spindler, and G.U. Nienhaus. 2002. A far-red fluorescent protein with fast maturation and reduced oligomerization tendency from *Entacmaea quadricolor* (Anthozoa, Actinaria). *Proc. Natl. Acad. Sci. USA.* 99:11646–11651. doi:10.1073/pnas.182157199

Williams, T., and J.E. Brenman. 2008. LKB1 and AMPK in cell polarity and division. *Trends Cell Biol.* 18:193–198. doi:10.1016/j.tcb.2008.01.008